Astronomy & Astrophysics manuscript no.
(will be inserted by hand later)

The Westerbork HI Survey of Spiral and Irregular Galaxies II. R-Band Surface Photometry of Late-type Dwarf Galaxies⋆

R. A. Swaters[1,2,3] and M. Balcells[4,1]

[1] Kapteyn Astronomical Institute, P.O. Box 800, 9700 AV Groningen, The Netherlands
[2] Dept. of Physics and Astronomy, Johns Hopkins University, 3400 N. Charles Str., Baltimore, MD 21218, U.S.A.
[3] Space Telescope Science Institute, 3700 San Martin Drive, Baltimore, MD 21218, U.S.A.
[4] Instituto de Astrofísica de Canarias, E-38200 La Laguna, Tenerife, Spain

Received date; accepted date

Abstract. *R*-band surface photometry is presented for 171 late-type dwarf and irregular galaxies. For a subsample of 46 galaxies *B*-band photometry is presented as well. We present surface brightness profiles as well as isophotal and photometric parameters including magnitudes, diameters and central surface brightnesses. Absolute photometry is accurate to 0.1 mag or better for 77% of the sample. For over 85% of the galaxies the radial surface brightness profiles are consistent with published data within the measured photometric uncertainty. For most of the galaxies in the sample HI data have been obtained with the Westerbork Synthesis Radio Telescope. The galaxies in our sample are part of the WHISP project (Westerbork HI Survey of Spiral and Irregular Galaxies), which aims at mapping about 500 nearby spiral and irregular galaxies in HI. The availability of HI data makes this data set useful for a wide range of studies of the structure, dark matter content and kinematics of late-type dwarf galaxies.

Key words. Surveys – Galaxies: dwarf – Galaxies: photometry

1. Introduction

Over the years, a growing body of CCD-based data on the surface brightness distributions of spiral and dwarf galaxies has become available (e.g., de Jong & van der Kruit 1994; Courteau 1996; Frei et al 1996; Heraudeau & Simien 1996; Patterson & Thuan 1996; Tully et al 1996; Matthews & Gallagher 1997; Peletier & Balcells 1997; Jansen et al 2000). CCD imaging has been the impetus for many new studies of a range of aspects of disk galaxies, such as general scaling laws (de Jong 1996a; Courteau et al 1996; Graham & Prieto 1999; Jansen et al 2000), the vertical light distribution (de Grijs & van der Kruit 1996; de Grijs 1998), the presence of thick disks (Sackett et al 1994; van Dokkum et al 1994; de Grijs & Peletier 1996), the radial truncation of the light distribution (Pohlen et al 2000; de Grijs et al 2000), asymmetries and lopsidedness (Rix & Zaritsky 1995; Zaritsky & Rix 1997; Kornreich et al 1998; Conselice et al 2000), and the stellar populations of disk galaxies (de Jong 1996b; Peletier & Balcells 1996; Bell & de Jong 2000).

A combination of optical imaging data with HI observations, which provide information both on the distribution of HI and on the kinematics of these galaxies, is a powerful tool to further our understanding of the properties of disk galaxies, as has been demonstrated by numerous papers in the literature in which one or a few galaxies are discussed. To date, however, there does not exist in the literature a large sample of galaxies for which both photometry and HI imaging exists. The ongoing Westerbork HI survey of spiral and irregular galaxies (WHISP), which aims at mapping about 500 spiral and irregular galaxies in HI, is well suited for a more statistical study of the link between optical and kinematical properties of disk galaxies (for more details on the WHISP project and its goals, see Swaters et al 2000, hereafter Paper I).

The two main aspects of the WHISP survey are a study of the HI component of galaxies in itself, and a study of the kinematic properties, focussing on rotation curves and dark matter properties. As part of the WHISP survey, optical *R*-band images have been obtained for the galaxies in the WHISP sample. These optical data provide the deep

⋆ Based on observations made with INT operated on the island of La Palma by the Isaac Newton Group in the Spanish Observatorio del Roque de los Muchachos of the Instituto de Astrofisica de Canarias. The tables in Appendix A are only available in electronic form at the CDS via anonymous ftp to cdsarc.u-strasbg.fr (130.79.128.5) or via http://cdsweb.u-strasbg.fr/cgi-bin/qcat?J/A+A/ The figures in Appendix B are only available in electronic form http://www.edpsciences.org

optical images and accurate optical global properties, such as disk surface brightnesses, disk scale lengths, integrated magnitudes and optical diameters that are needed for a detailed comparison of the optical, HI and dark matter properties. In addition to the two main aspects of WHISP, the combination of the HI distribution, the kinematics and the light distribution will allow detailed studies of the nature of for example scaling laws between HI and optical properties, warps, truncated disks, and lopsidedness.

In this paper, we present optical surface photometry data for the 171 late-type dwarf galaxies in the WHISP sample. The outline of the paper is as follows. Sect. 2 describes the selection of the sample. In Sect. 3 the distance uncertainties for the dwarf galaxies in our sample are discussed. Sect. 4 describes the observations and the data reduction steps. In Sect. 5 the ellipse fitting used to derive the surface brightness, ellipticity and position angle profiles is described. Sect. 6 presents the global photometric parameters obtained from the data, and Sect. 7 describes the internal checks on our surface photometry, the comparison of our profiles to those of other authors and the comparison of global parameters to catalog values. Sect. 8 gives a brief description of the optical properties of the galaxies in this sample. Finally, Sect. 9 gives a summary of the main results.

To facilitate the reading of text and tables, all long tables have been placed at the end of the paper. Appendix A presents the tables with the selected sample, the assumed distances for all galaxies, the list of observations and the derived optical properties. Grayscale representations of each galaxy, together with surface brightness profiles, are given in Appendix B.

2. Sample

The late-type dwarf galaxies presented here are part of the much larger WHISP sample. This sample has been selected from the Uppsala General Catalogue of Galaxies (UGC, Nilson 1973), and it consists of all UGC galaxies with a blue major-axis diameter larger than $1.5'$, $\delta(2000) > 20°$, and an HI line flux density larger than 100 mJy (as calculated from the ratio of total HI fluxes and profile widths as listed in the Third Reference Catalogue of Bright Galaxies (hereafter RC3, de Vaucouleurs et al 1991)). These criteria ensure sufficient resolution and a high enough signal-to-noise ratio for observation with the Westerbork Synthesis Radio Telescope.

From the WHISP sample all late-type dwarf galaxies were selected for the present study. The sample consists of two subsamples. The first consists of galaxies with HI flux densities above 200 mJy, that either have morphological types later than Sd, or that have earlier morphological types and are fainter than $M_B = -17$. This subsample contains 113 late-type dwarfs and forms the basis of a study of HI and dark matter in late-type dwarf galaxies (see Swaters 1999). The second subsample comprises 80 galaxies with flux densities between 100 and 200 mJy that were classified as dwarf galaxies by Nilson (1973). The total sample constructed in this way contains 193 galaxies. No upper limit was set for the diameter of the selected galaxies. For the 200 mJy sample, no lower limit to the diameter was applied either, which resulted in the inclusion of four dwarf galaxies with blue major-axis diameters smaller than $1.5'$. Furthermore, there was no selection criterion based on the environments of these dwarfs. Isolated dwarfs as well as dwarf companions to larger galaxies have been included in the sample.

Besides the selection effects of the UGC, which are well studied (Thuan & Seitzer 1979; Paturel et al 1991; de Jong & van der Kruit 1994), the present sample has an additional selection effect as a result of the requirement that the galaxies have HI measurements listed in the RC3. Not all galaxies have been observed in HI (57% of the galaxies that meet all our criteria except the flux density criterion have a measured HI flux listed in the RC3), and those that have been observed come from studies with different scientific goals, different telescopes and different sensitivities. In addition, the selection based on the flux density may introduce a dependency on the inclination and the kinematic properties of the galaxies. Therefore the true selection function is difficult to quantify. With these caveats in mind, the sample is representative of this galaxy population as it spans the entire range of properties of late-type dwarfs.

Because morphological type was one of the main selection criteria for the sample selection, a few galaxies were included in the sample that were assigned late morphological types, but that proved not to be dwarf galaxies but large irregular galaxies, such as interacting systems and peculiar galaxies. Though these will be excluded in later studies of the properties of late-type dwarfs, their optical properties are presented here.

The sample of observed galaxies is listed in Table A.1. Out of the total of 193 galaxies, 171 have been observed. The remaining 22 have been missed due to bad weather. The galaxies in the 200 mJy sample were given priority, as a result only 2 out of the 113 galaxies in that sample have not been observed.

3. Galaxy distances

An important source of uncertainty for mass models of our dwarf sample are the galaxy distances. Care has been given to using the best distance estimator available for each galaxy. Here we discuss the choice of distance estimators and the magnitude of the distance uncertainty associated to each.

The distances for the late-type dwarf galaxies in our sample have been obtained from a search of the literature up to and including 1998. Most of the literature distances have been derived from four distance indicators. In order of decreasing priority these are based on Cepheids, brightest stars, group membership and systemic velocity. A full list of the adopted distances for all of the galaxies in our sample, including the method used to determine the distance, is given in Table A.2. Unfortunately, Cepheid

distances are available for only three of the galaxies in our sample. Below the uncertainties for the three other methods are discussed.

3.1. Brightest stars

The accuracy of the brightest star method to determine the distance has been subject of many discussions. There are a number of possible problems, in particular if the brightest blue stars are used (e.g., Humphreys & Aaronson 1987). The brightest stars in a galaxy may not be individual stars, but star clusters or compact HII regions, or these stars may be variable. In addition, it is found that the luminosity of the brightest stars is dependent on the luminosity of their parent galaxy, thus introducing a degeneracy in the distance determination (e.g., Humphreys 1983). The brightest red stars suffer much less from these problems.

The reported accuracy of the brightest stars as distance indicators differs substantially between different studies. Rozanski & Rowan-Robinson (1994) found that the uncertainty in the distance modulus is 0.58 mag for the brightest red stars and 0.90 mag for the brightest blue stars. Karachentsev & Tikhonov (1994), on the other hand, find uncertainties of 0.37 mag and 0.46 mag, respectively. Lyo & Lee (1997) found, from a comparison of distance determinations based on Cepheids and brightest stars, that the uncertainties in the distance moduli are 0.37 mag for the brightest red stars, and 0.55 for the brightest blue stars, and they conclude that the brightest red stars are therefore useful distance indicators.

Most of the distance determinations from brightest stars, listed in Table A.2, are based on brightest red stars. With an uncertainty in the distance modulus of 0.37 mag, the uncertainty in the distance is about 20%. If the uncertainty is as high as 0.58, as suggested by Rozanski & Rowan-Robinson (1994), the distance uncertainty will be about 30%.

3.2. Group membership

Distances from group membership are mostly based on the groups identified in de Vaucouleurs (1975) and de Vaucouleurs et al (1983). The published distance moduli for these groups were derived from several distance indicators: (a) from optical tertiary indicators (morphological type and luminosity class); (b) from the mean redshift of the group and a position-dependent Hubble constant (varying between 70 km s^{-1} Mpc^{-1} and 110 km s^{-1} Mpc^{-1}), calibrated with spiral galaxies whose distances were determined from tertiary distance indicators; (c) from the Tully-Fisher relation. Unfortunately, de Vaucouleurs et al (1983) do not list which particular distance indicator or combination of distance indicators was used to obtain the distance modulus they list. For the details on these distance indicators, see de Vaucouleurs et al (1983) and references therein.

Given how the group membership distances have been determined, it is clear that these distance may suffer from substantial uncertainties. De Vaucouleurs (1979) claims that the uncertainty in the distance moduli obtained from tertiary distance indicators is less than 0.4 mag. The Hubble constant based on tertiary distance indicators has an average value of about 90 km s^{-1} Mpc^{-1}, higher than the currently favored value of the Hubble constant, which may indicate that the tertiary distance indicators tend to underestimate the distance.

Adding to this uncertainty is the fact that at small distances the depth of the group may be a significant fraction of the group distance.

3.3. Systemic velocity

For all the galaxies in our sample a distance was calculated from the HI systemic velocity following the prescription given in Kraan-Korteweg (1986) to correct for Virgocentric flow, with an adopted Hubble constant of 75 km s^{-1} Mpc^{-1}. Many of the dwarf galaxies have low systemic velocities, and these may well be dominated by peculiar motions. As a result, these distances derived from the systemic velocities may have large uncertainties, in particular for the closest galaxies.

3.4. Comparison of distances

In the top panels of Fig. 1 the comparison between the distances derived with the three different methods is shown. In Fig. 1a the distances derived from the HI systemic velocities and group memberships are compared. Two features stand out. Firstly, at small distances there are a number of points that are grouped along slanted lines. These arise because there are a number of large nearby groups to which a substantial number of dwarfs are assigned, such as the M81 group, the M101 group and the NGC 4736 group. Secondly, at larger distances there appears to be a systematic difference between the group distance and the distance derived from the systematic velocity, in the sense that the group distances are generally smaller. This may be the result of an underestimate of the distances determined from tertiary distance indicators, as mentioned above. On the other hand, almost all of these galaxies are in the same region of the sky as the Virgo cluster. In this direction, the relation between the systemic velocity and the distance is less certain. This may also contribute to the differences between the two distance estimates compared in Fig. 1a.

Fig. 1b shows a comparison of the distance from the HI systemic velocity and the brightest star distance. There appears to be a weak correlation between these two distance estimates. Towards smaller HI distances, the ratio of HI distance over brightest star distance decreases. All of the galaxies for which brightest star distances are available are, because of the nature of the method, at small

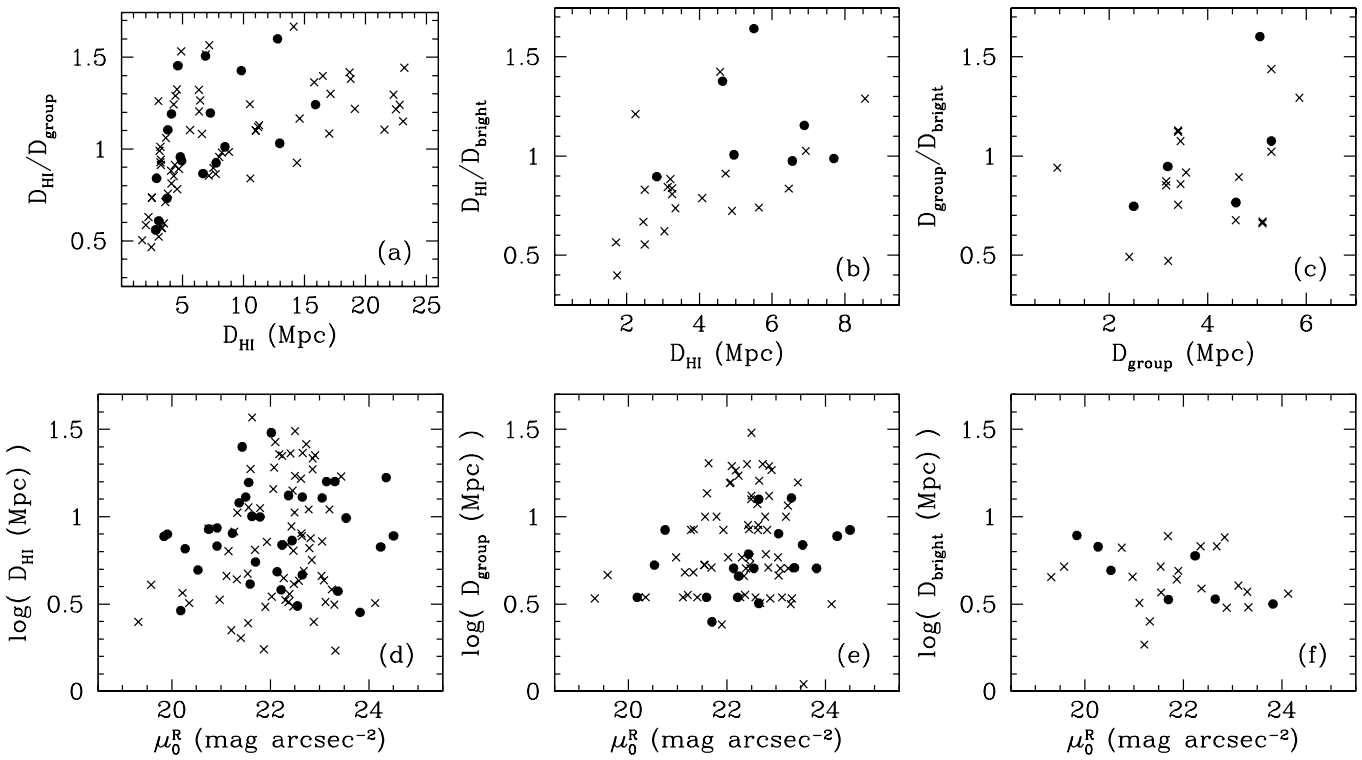

Fig. 1. (a-c) Ratios of distances derived from different distance indicators, plotted against the derived distances. The distances based on the HI systemic velocities are represented by $D_{\rm HI}$, $D_{\rm group}$ refers to the group membership distances, and $D_{\rm bright}$ to the distances derived from the brightest stars. **(d-f)** Derived distances versus R-band central disk surface brightness μ_0^R.

distances. At such small distances, the distances as derived from the HI systemic velocities are uncertain.

In Fig. 1c the group distances are compared with the brightest star distances. There is a slight indication that the average ratio plotted in Fig. 1c is below unity, indicating that distances based on group membership are smaller than those based on brightest stars, similar to what was concluded from Fig. 1a.

Another concern is that the distance estimates may depend on the surface brightness of the galaxies. Although this is unlikely for the distances derived from the HI systemic velocities, it may play a role for the group membership distances, which are partially based on tertiary distance indicators, and for the brightest star distances. In Fig. 1d-f the different distance estimates are plotted against central disk surface brightness μ_0^R. There does not appear to be a correlation between surface brightness and the HI distance (Fig. 1d), nor is such a correlation evident in (Fig. 1e, in which the group distance is plotted versus surface brightness.

Finally, at best a weak trend is seen between the brightest star distance and the surface brightness. The variations from low to high surface brightness are about 25%, comparable to the random errors. For low surface brightness galaxies smaller distances are found. Because of the lack of a precise distance indicator, it is unclear what causes this trend. It may be a result of selection effects. On the other hand, it may also be that the magnitudes of the brightest stars depend on surface brightness.

In summary, there are some indications that the group membership distances may underestimate the true distances. This systematic difference appears to be no larger than about 20%. In addition, the distance estimates based on brightest stars may depend on surface brightness, but these effects are probably smaller than 25%. This possible systematic error is likely to be dominated by the random errors in the distance estimates. Based on Figs. 1a-c, we estimate that the largest uncertainty in distance is about 60%, and that the typical distance uncertainty is about 30%.

4. Observations and data reduction

As mentioned in the introduction, one of the usages of the optical data is to provide the stellar distribution for mass modeling. For the light distribution to be close to the stellar mass distribution, observations at red wavelengths are necessary to minimize the effects of extinction and young populations. I-band observations were not suitable because of the brighter sky in I, making longer exposures necessary, and because of fringing making accurate flatfielding difficult. Even longer wavelengths, such as the K-band, were not practical because the available infrared arrays had too small a field of view for the galaxies in the sample. This would make mosaicking necessary and therefore require a lot of observing time. The R-band offered the best compromise. A possible problem in using R-band is that the Hα emission line is included in the

Table 1. List of observing runs

May 1 – May 6, 1994 (m94)
November 29 – December 4, 1994 (d94)
February 2 – February 6, 1995 (f95)
May 27 – May 28, 1995 (m95)
December 23 – December 28, 1995 (d95)
May 10 – May 15, 1996 (m96)

wavelength range covered by this filter. Jansen (2000) has found that the median contribution of Hα to the R-band flux is 2.0% for late-type dwarf galaxies, with a maximum of 8%. Gallagher & Hunter (1989) show that radial Hα profiles and the R-band radial surface brightness profiles have similar shapes. Hence, we expect that the Hα emission may introduce a systematic offset from the true radial surface brightness profile of 0.02 mag on average, but the shape of the profile will hardly be affected.

We used the f/3.29 prime focus camera at the 2.54m Isaac Newton Telescope at La Palma, during six observing runs between May 1994 and May 1996. A list of the observing dates is given in Table 1. In all runs, we used Harris filters. In the May 1994 run, we used an EEV CCD, in all other runs we used a thinned Tektronix CCD (TEK3). Specific details on the CCDs used are given in Table 2, which lists the readout noise, gain, pixel size, chip size and field of view for each chip. The EEV chip was always used in standard readout mode, the TEK CCD was mostly used in quick readout mode, saving time on readout of the chip. The increased readout noise was not important because the exposures are limited by photon noise. The emphasis was to reach faint surface brightness levels. For this reason, most galaxies were observed only in the R-band. However, for 46 galaxies we have obtained B-band data, which are presented here as well.

Most galaxies were observed only once. Galaxies for which the center was found to be saturated were observed a second time with a shorter exposure. A list of all observations is given in Tables A.3 and A.4. Some galaxies were observed in different observing runs, and these data were used for internal comparison of the photometric accuracy. Only the data with the best photometric conditions are listed. All of the data processing was done in IRAF.

4.1. Bias subtraction

Both the EEV and the TEK3 had flat bias levels and low dark currents, but the bias level did tend to vary slightly during the night. Therefore, the bias level was determined from the overscan regions. The May 1995 and the December 1995 run showed random bands in the bias levels, which were visible throughout the image. The amplitude of these bands was about 1 to 2 counts. For these images, the bias level was removed by subtracting from each image row the average of the corresponding bias row.

4.2. Flat fields

The instrument was known to have light leaks at the filter wheel, causing some excess light at the edges of the images. By wrapping the prime focus cone unit in a dark cloth, this effect was almost entirely removed, allowing accurate flat fielding.

During all the runs, twilight flats were taken at the beginning and the end of the nights, typically with 10000 to 30000 counts. Additionally, for increased accuracy night sky flats of blank fields were taken, typically seven per filter (each exposure 180 seconds in R and 300 in B).

For each night and filter we constructed a set of flat fields, by combining in different ways the twilight flats or the night sky flats. When more than two flat fields were combined, a rejection algorithm was used to remove stellar images and cosmic-ray events. Otherwise, stars and cosmic-ray events events were edited out by hand and replaced by the local average. Night sky flats were offset from one exposure to the other, so that stars could be filtered out. This filtering proved to be satisfactory under good seeing conditions ($< 1.5''$) with 6 or 7 exposures. When the seeing was worse, or when fewer exposures had been obtained, stellar residuals remained in the constructed flat field. In the latter case, flat fields were constructed by fitting a low order two-dimensional polynomial to the night sky flat and to the twilight flat; next, the twilight flat was divided by its fit, thus obtaining the high signal-to-noise small scale variations, and these were multiplied into the fit to the night sky flat.

After constructing these flat fields, a number of exposures of each night was flat fielded by each of the constructed flatfields in order to test which provided the most accurate results. This was done by checking the flatness of the empty regions. In more than half of the cases the night sky flat fields allowed more accurate flat fielding than the twilight flats.

Because of this careful construction and testing of the flatfields, high flatfield accuracy was obtained. For each exposure the sky values at four places around each galaxy were measured, carefully avoiding the outer parts of the galaxy and the halos of bright stars. The background flatness was taken to be half the difference between the minimum and maximum values. The flatness defined in this way has a median value of 0.22% for the sample in R, and 0.32% in B.

4.3. Calibration

At regular intervals during each night, standard star fields from Landolt (1992) were observed. The fields we used were RU 149, PG0231+051, PG0942-029, PG1323-086, PG1525-071, PG1528+062 and PG 2213-006. With these stars and the magnitudes given in Landolt (1992), the observations were calibrated to Johnson B and Kron-Cousins R. The standard stars were observed over a range of airmasses for both bands, both on photometric and non-photometric nights. For all these stars we determined

Table 2. CCD characteristics

CCD	Readout	Gain	Noise (e)	Pixel size ($''$)	CCD size	Field of view
EEV	standard	0.69	3.9	0.55	1280x1180	$11.4' \times 10.5'$
TEK	standard	0.73	4.7	0.59	1124x1124	$10.0' \times 10.0'$
TEK	quick	1.47	6.2	0.59	1124x1124	$10.0' \times 10.0'$

Table 3. Calibration coefficients

Run	night	$c_{1,R}$	$c_{2,R}$	$c_{1,B}$	$c_{2,B}$
May 94	1	-0.480	0.196	0.697	0.223
	2	-0.489	0.160	—	—
	3	-0.510	0.184	—	—
	4	-0.462	0.149	0.564	0.287
	5	-0.448	0.145	—	—
	6	-0.591	0.285	—	—
Dec 94	1	-0.238	0.104	—	—
	4	-0.106	0.090	—	—
	5	-0.163	0.080	—	—
	6	-0.171	0.092	0.020	0.221
Feb 95	1–5	-0.16	0.09	-0.19	0.37
May 95	1	0.116	0.035	0.361	0.175
	2	0.102	0.064	0.389	0.175
Dec 95	1	-0.172	0.086	0.004	0.227
	2	-0.237	0.155	0.125	0.196
	3–6	-0.151	0.155	0.109	0.220
May 96	1	-0.061	0.104	-0.076	0.316
	2	-0.094	0.101	-0.056	0.263
	4	-0.091	0.123	-0.104	0.322

the instrumental aperture magnitudes and spurious values were deleted. These data were combined to fit zero-point magnitudes and color and extinction coefficients of the form:

$$\begin{aligned} b &= B + c_{1,\,B} - 25 + c_{2,B}\,X + c_{3,B}\,(B-R) \\ r &= R + c_{1,\,R} - 25 + c_{2,R}\,X + c_{3,R}\,(B-R) \end{aligned} \qquad (1)$$

where B and R are the standard star magnitudes, b and r are the instrumental magnitudes, X is the airmass, c_1 is the zero-point offset, c_2 is the airmass term, and c_3 is the color term. The color terms were found to be small, and can be neglected. For most galaxies only R-band data are available, but the missing color information does not significantly affect the accuracy of the calibration.

The calibration was done for each night independently, except for a few nights with poor photometric conditions, for which a combined calibration was done. The derived calibration coefficients are listed in Table 3. The 1σ residuals of the fit given by Eq. (1) give the uncertainty on the calibration, and are listed in Tables A.3 and A.4 for the R and B-band, respectively. This uncertainty also includes the uncertainty introduced by ignoring the color term. During nights with cirrus, standard stars were observed as well and obviously, the resulting photometric uncertainties are large. For those galaxies for which more than one observation was available, we used the one with the best photometry. If the seeing of the non-photometric observations was better, or if that image had a higher signal-to-noise ratio than the photometric one, we used the latter to calibrate the non-photometric observation.

The majority of the sample has good photometric accuracy. The zero point uncertainty is less than 0.1 mag for 77% of the sample, and below 0.2 mag for 89% of the sample.

4.4. Image combination

All exposures of the same galaxy observed in the same run were aligned using stars common in the frames. If more than two exposures were available, the images were combined using a rejection algorithm to remove cosmic-ray events. Otherwise, the cosmic-ray events were removed using the FIGARO BCLEAN algorithm privately ported to IRAF and replaced with the local average. If the central parts of a galaxy were saturated in a long exposure, the saturated pixels were rejected during the image combination and replaced with scaled values from the short exposure images.

A few galaxies were too large to fit in the $10' \times 10'$ field of view. These galaxies were mosaicked. All galaxies to be mosaicked were observed in the December 1995 run, under poor photometric conditions. The sky for all the images was subtracted and the images were aligned using stars in overlapping regions. Next, the images were scaled to the same exposure time, and scaled photometrically to the frame with the lowest sky and the highest counts per second, and the images were combined.

4.5. Final steps

In each frame the mean value of the sky was determined in four areas near the galaxy that were free of objects, stellar halos and scattered light. The sky value for each frame was the average of these four mean values. For the estimate of the uncertainty in the sky determination we used half the difference between the minimum and the maximum of the four mean values. This estimate of the uncertainty in the sky includes large scale variations in the flat fielding and also the uncertainty in the sky determination itself.

For each exposure the seeing was estimated by fitting two-dimensional Gaussians to all objects in the field that had been masked by hand (see Sect. 5). Only objects with

ellipticities smaller than 0.15 and central peaks more than five times the noise were used, to avoid contamination by background galaxies and inaccurate measurements. On average, about 40 objects were used to obtain the seeing estimate. The seeing estimates listed in Tables A.3 and A.4 are the median values of the individual fits. Given the pixel size of about $0.6''$, the observations with the best seeing are undersampled. This affects approximately 15% of the data presented here.

The last step was to add the coordinate system to the frames. The coordinate system was transferred from the Digitized Sky Survey (DSS), by determining coordinates from the plate solution for stars visible in both the DSS and the CCD image. Using these coordinates, a coordinate system was fitted to the CCD frame, using about ten stars. We used a four term matrix to describe the coordinate system in a gnomonic projection. The 1σ errors on the coordinate system determined in this way are about $0.5''$. This is comparable to the typical error of $0.6''$ found by Veron-Cetty & Veron (1996). The R-band images of all galaxies, including the coordinate system, are presented in Appendix B.

5. Isophotal fits

Fitting ellipses to late type dwarf galaxies is not straightforward. Often, the light distribution is irregular, and sometimes a well defined center is missing, or the centers for the inner and outer parts are different. Nonetheless, the radial surface brightness profile gives a useful representation of the light distribution.

Before fitting ellipses to the galaxy images, we masked out all the stars and the scattered light in the frames by hand. Special care was taken to mask out low intensity halos of stars as well. In some cases this proved impossible, due to the proximity of a bright star to the galaxy image. In these cases, the foreground light was masked out to where the galaxy light started to be dominant and the contribution of the stellar halo was incorporated in the uncertainty in the sky determination.

The ellipse fitting itself was done using the GALPHOT package (Franx et al 1989; Jørgensen, Franx & Kjægaard 1992). The ellipse parameters were determined at logarithmic intervals, each next ellipse having a radius 1.2 times bigger than the previous ellipse, with the innermost radius at $1''$. The radius r of each ellipse is defined as $r = \sqrt{ab}$, where a is the major axis and b the minor axis. The ellipticity is defined as $1 - b/a$. Determining the ellipse parameters was done in several steps. To make sure that the ellipse fits were not affected by substructure, HII regions, bars or other luminous components, all fits were individually inspected at each step in the process, and adjusted as described below when necessary.

First, we ran the fitting program leaving all the parameters (center, position angle and ellipticity) free. From these results we determined the center. If the galaxy had a well determined center, e.g. a nuclear peak or a clear central condensation, this was adopted to be its center. In most other cases, we determined the center from the average of the outer ellipses where the solution was more stable. In those cases where the outer parts were highly irregular, the center was determined from the average of the inner parts. The adopted center for each galaxy is indicated in Appendix B with a cross.

In the second step, the center was fixed. From these results we determined the position angle. This was done by averaging over the outer ellipses, over the region where the results were converging. The outermost points were discarded if these gave erratic results. If the position angle varied systematically with radius, the average position angle was used. For galaxies with a pronounced bar, we tried to determine the position angle of the surrounding disk.

In the third iteration, the center and position angle were fixed, in order to determine the ellipticity. We determined the value for the ellipticity in the same way as we determined the position angle. The ellipticities were set to zero if equal to zero within the uncertainties of the measurements.

After fixing the orientation parameters, we extracted the calibrated radial surface brightness profiles from all the images. The orientation parameters as found for the R-band were also used to extract the B-band radial surface brightness profiles. In Appendix B we show the radial surface brightness profiles and the exponential fits (see Sect. 6) for all galaxies. Also, the run of orientation parameters (center, ellipticity and position angle) with radius are presented. Note that these have been derived from the free fits and may therefore, in some cases, deviate substantially from the values chosen from subsequent fits with more parameters fixed.

6. Structural parameters

6.1. Profile fitting

Most of the radial surface brightness profiles are smooth and regular, despite the often irregular optical appearance of the galaxies. Some show a central excess of light, while others have a central flattening. In this paper, we have not attempted to make decompositions into disk and central components. Instead, we focused on the disk component in these galaxies. An exponential intensity law was fitted to the outer parts of the profiles, which becomes a linear relation when expressed in magnitudes:

$$\mu(r) = \mu_0 + 1.0857\,\frac{r}{h}, \qquad (2)$$

where μ_0 is the extrapolated central disk surface brightness, and h is the disk scale length. The photometric errors were used as weights. Combined with the logarithmic spacing of the points in the profile, this leads to higher weights to the central parts. Most of the profiles are well described by an exponential. The profiles and their fits are shown in Appendix B. In a later paper, we will study the properties of the galaxies with central light concentrations with the use of the Sersic profile (Sersic 1968).

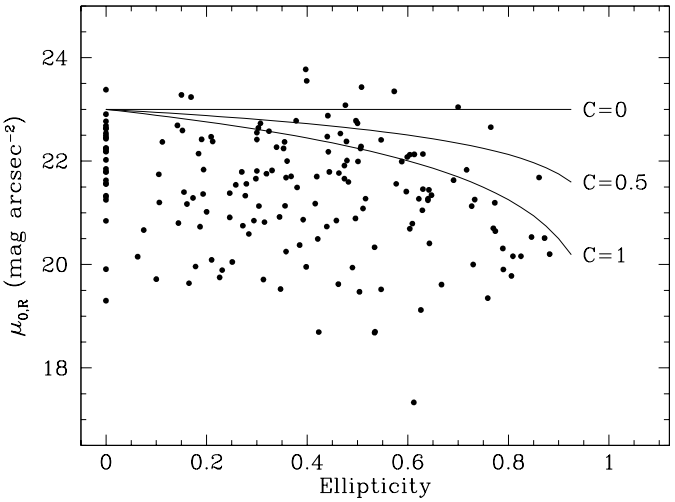

Fig. 2. R-band central disk surface brightness $\mu_{0,R}$ versus ellipticity. The solid lines defined by Eq. (3). $C = 0$ corresponds to optically thick, $C = 1$ to optically thin.

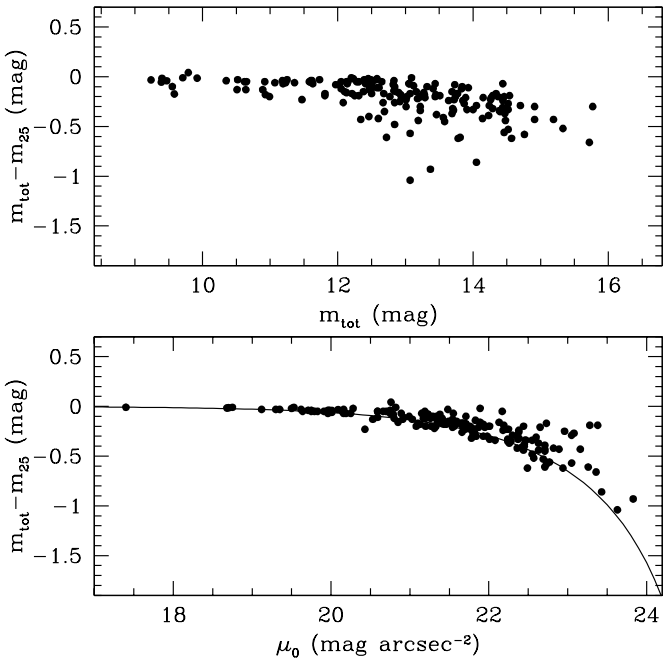

Fig. 3. The extrapolation from m_{25} to $m_{\rm tot}$ versus the integrated magnitude $m_{\rm tot}$ (*top panel*) and versus the extrapolated central disk surface brightness μ_0 (*bottom panel*). The solid line represents the correction for a purely exponential disk (see text).

6.2. Observed central surface brightness

Beside the extrapolated central disk surface brightness μ_0 derived from the fit, we also determined the observed central surface brightness, μ_c. This value differs from μ_0 if the profile shows a central peak or flattening. The observed central surface brightness μ_c was determined from a linear extrapolation of the surface brightness profile in the inner few arcseconds to $r = 0$. This is justified given the exponential shape of the inner profile in most cases, also for profiles with a central concentration of light.

6.3. Diameters

For each galaxy two sets of diameters have been determined. Isophotal diameters in both the R and the B-band have been determined at $\mu_R = 25$ and 26.5 mag arcsec^{-2}. Additionally, effective radii within which 20%, 50% and 80% of the light is contained have been calculated.

6.4. Extinction and inclination corrections

The observed surface brightnesses and magnitudes suffer from extinction, both from dust in our Galaxy and from that internal to the observed galaxy. The data were corrected for Galactic extinction using the values for A_B from Burstein & Heiles (1984). The values for A_R have been obtained assuming an A_B/A_R of 1.77 (Rieke & Lebofsky 1985).

The correction for internal extinction is less certain. A relationship is expected between the axis ratio b/a and the observed surface brightness μ_0 of approximately:

$$\mu_0 = \mu_0^i + 2.5\, C \log (b/a), \qquad (3)$$

where μ_0^i is the surface brightness corrected for inclination, and where C is a constant related to the extinction. For the transparent case, C is equal to unity, for the opaque case it is zero.

The dependence of μ_0 on b/a is shown in Fig. 2. Note the relative paucity of high inclination, low surface brightness galaxies. This might indicate that the galaxies in this sample are transparent, and it would imply a lower cutoff in the true surface brightness distribution of dwarf galaxies at $\mu_{0,R} = 23$ mag arcsec^{-2}. However, the lack of such galaxies may well be the result of selection, e.g. as a result of the selection on flux density. In addition, given the selection on morphological type, some galaxies may drop out of our sample if they may have been misclassified as earlier morphological types when seen edge-on. The latter could contribute to the lack of high surface brightness edge-on galaxies that are expected in the optically thin case. In any case, any expected trend is weak because of the wide range in surface brightnesses at each b/a. Also, the correction is uncertain in the cases where the ellipticity varies with radius. In conclusion, Eq. (3) does not provide a useful way to determine the transparency for this sample of galaxies.

Because dwarf galaxies generally have low metalicities (e.g., Skillman et al 1989), the dust content is likely to be low, and therefore these galaxies are expected to have small internal extinction. Therefore, $C = 1$ was adopted, and in the remainder of this paper the surface brightnesses were corrected accordingly. In the optically thin case, the integrated magnitudes do not need to be corrected. Note that the surface brightnesses and diameters listed in Tables A.5 and A.6 have only been corrected for Galactic extinction, not for inclination.

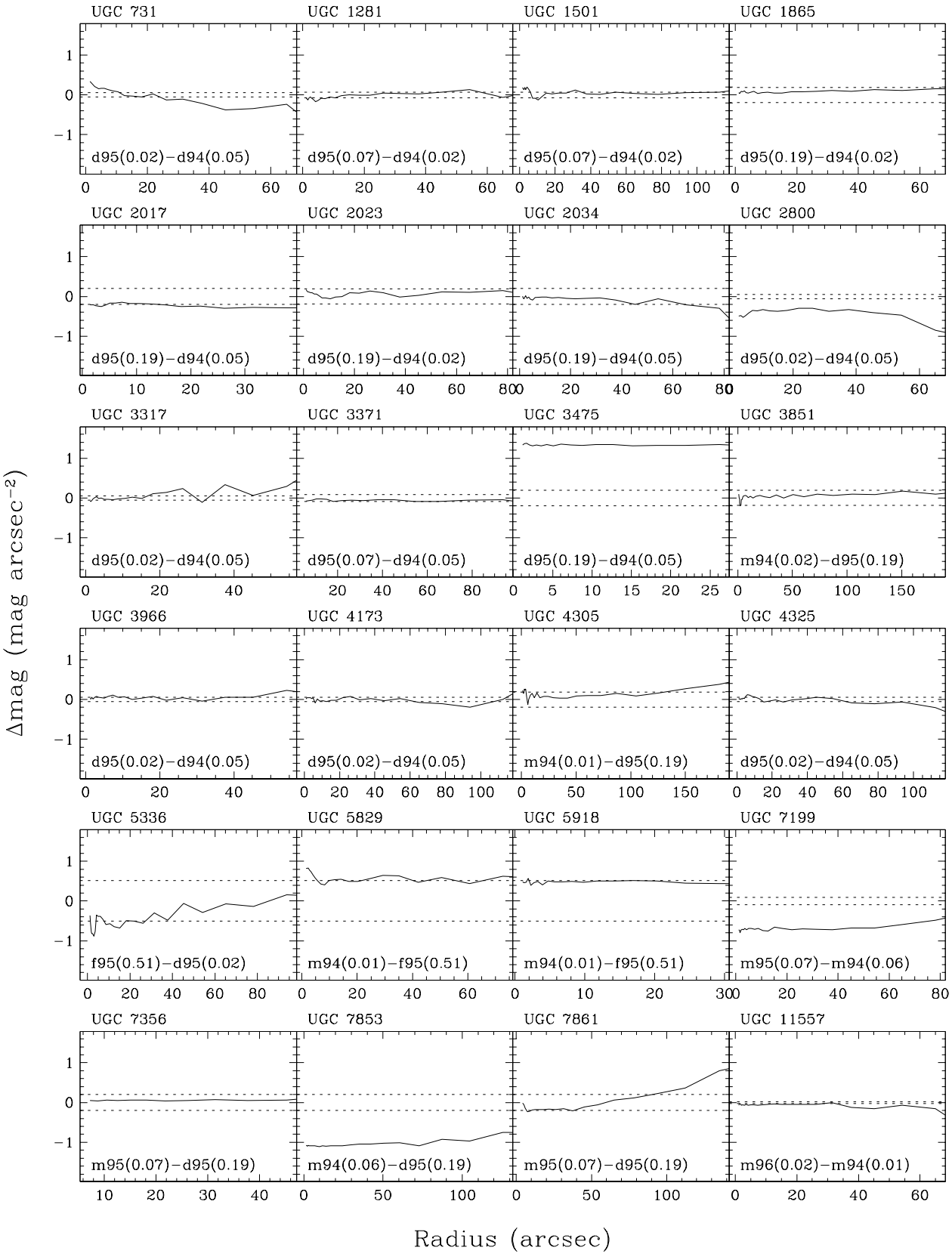

Fig. 4. Internal comparison for the R-band observations. The radial range for the comparison is set by the radius at which the profile with the largest uncertainty reaches 3σ above sky. At the bottom of each panel the observing runs that are compared are given, the number between brackets gives the photometric accuracy. The dotted lines in each panel give the combined 1σ errors. The shorthand used to refer to the observing runs is explained in Table 1.

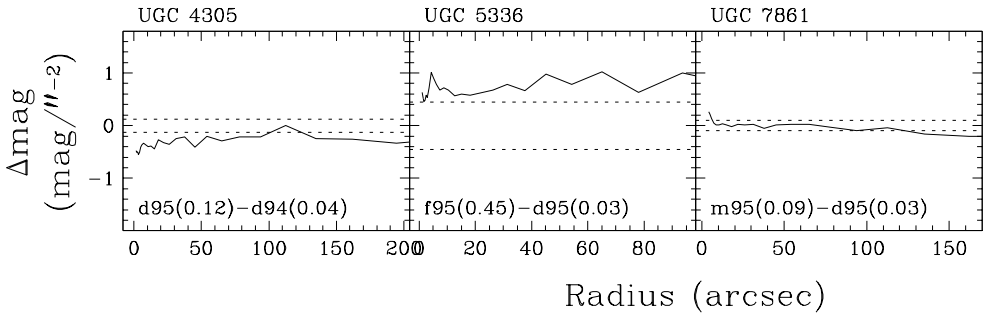

Fig. 5. Same as Figure 4, but for the B-band observations.

6.5. Integrated magnitudes

Three magnitudes have been determined for each galaxy, two isophotal (m_{25} and $m_{\rm lim}$) and one total magnitude ($m_{\rm tot}$). The isophotal magnitudes are calculated at two different levels. One at the 25 R mag arcsec^{-2}, and one at the limiting surface brightness level, which corresponds to the 3σ above sky level. The total magnitude has been calculated by extrapolating an exponential fitted to the outer parts of the surface brightness profile out to infinity. In particular for galaxies with low surfaces brightnesses, such as the dwarfs in this sample, this extrapolation can be significant. To first order, the extrapolation can be determined by assuming that the entire profile follows an exponential decay, as was done by Tully et al. (1996). However, applying such a correction overestimates the total magnitude when a central condensation is present, and underestimates it when the light profile flattens towards the center, as Tully et al (1996) already noted. To avoid this problem, we used the more general method to determine the total magnitude (Han 1992). This method assumes that the light falls exponentially outside the last point in the profile, but it makes no assumptions on the shape of the inner profile:

$$m_{\rm tot} = m_{\rm lim} - 2.5\log\left\{1+\frac{b}{a}\,q\Big(\frac{r_{\rm lim}}{h'}\Big)\,10^{-0.4(m_{\rm t}-m_{\rm lim})}\right\}, \quad (4)$$

where the function $q(x)$ reflects the luminosity-radius relationship for such an exponential disk,

$$q(x) = (1+x)\,e^{-x}, \quad (5)$$

$r_{\rm lim}$ is the radius where 3σ is reached, and

$$m_{\rm t} = \mu_0' - 5\log h' - 2.5\log 2\pi \quad (6)$$

is the total magnitude of a pure exponential disk characterized by μ_0' and h', as determined from fitting to the outer parts of the profile.

The top panel of Fig. 3 shows the extrapolation from m_{25} to $m_{\rm tot}$ versus the total magnitude $m_{\rm tot}$. The corrections become larger for less luminous galaxies, and may reach up to one magnitude. The bottom panel of Fig. 3 shows the extrapolation versus μ_0. The correction becomes larger for fainter surface brightnesses. The solid line shows the extrapolation for a purely exponential disk. The corrections generally follow this line closely. However, some points deviate up to about 0.5 mag from this line. This plot shows that just applying an extrapolation based on the assumption that the light profile is exponential may give total magnitudes that are significantly too bright, in particular for low surface brightness galaxies.

7. Comparison of radial surface brightness profiles

In order to assess the photometric quality of our data and to check the reliability of our estimate of the photometric uncertainty, radial surface brightness profiles of identical galaxies obtained during different runs have been compared. Our data have been compared to data available in the literature as well.

7.1. Internal comparison

Some galaxies were observed on more than one night. Although for each galaxy only one observation is given in this paper, these multiple observations have been used to assess the quality of our calibration. Figs. 4 and 5 show the internal comparison for the R and the B-band respectively. The dotted lines indicate the $\pm1\sigma$ range based on the uncertainties on the photometric solution. The majority of the profiles are equal within the uncertainties of the measurements. Five cases, UGC 2800, UGC 3475, UGC 7199, UGC 7853 and UGC 7861 deviate more than expected from our estimates of the uncertainty in the photometry. These galaxies were all observed on nights during which there was some cirrus present. The uncertainty caused by cirrus is in principle included in the photometric uncertainty. The deviant cases are probably the result of somewhat thicker cirrus clouds passing overhead occasionally. Because in 83% of the internal comparisons the photometric uncertainty is accurately known, including nights with some cirrus, we conclude that the photometric uncertainty we have derived is a reliable estimate of the real photometric uncertainty. The comparison for the B-band profiles, though available for only three galaxies, is consistent with this conclusion. Nights with cirrus have been

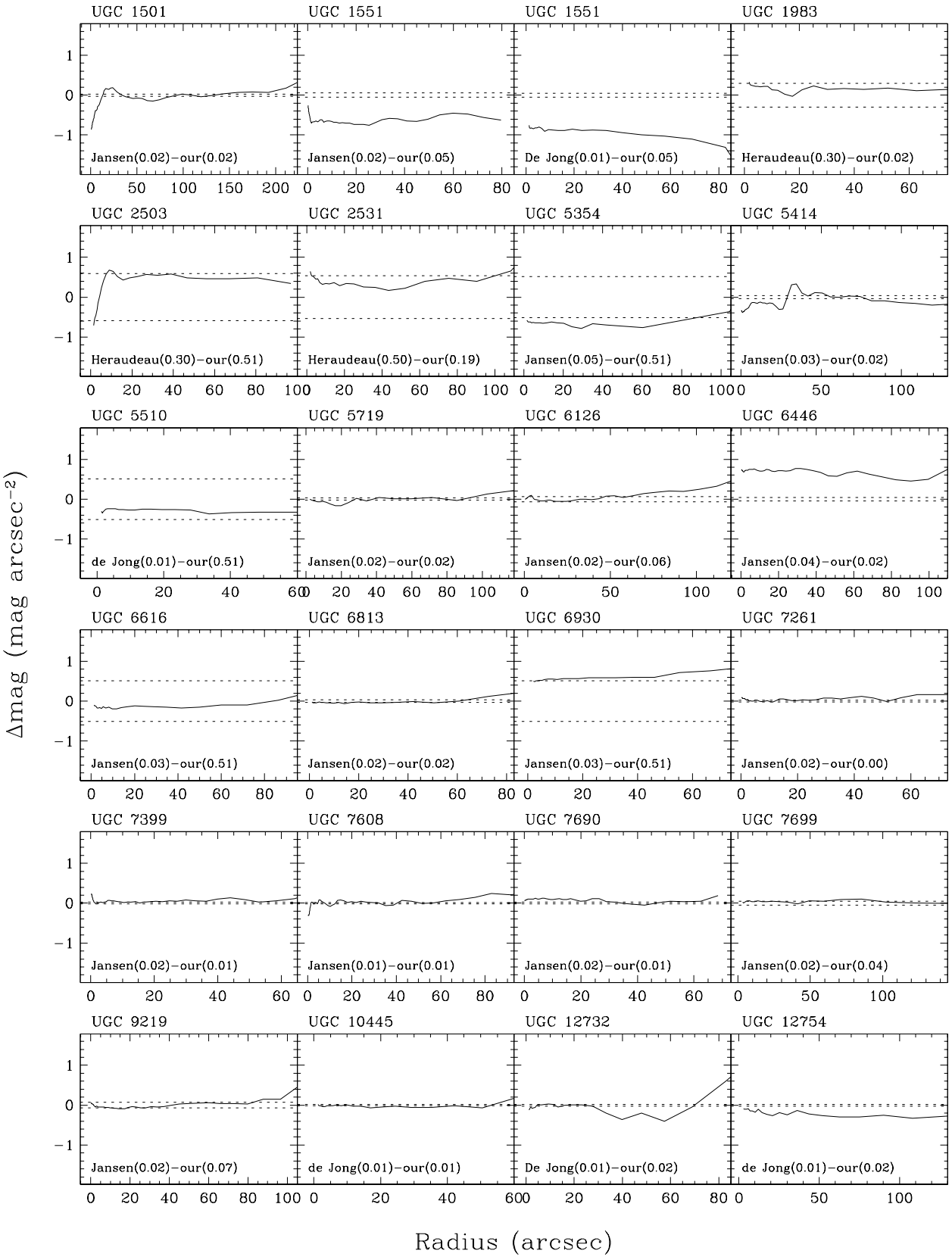

Fig. 6. External comparison for R-band observations. The radial range for the comparison is set by the radius at which the profile with the largest uncertainty reaches 3σ above sky. At the bottom of each panel the data that are compared are given, the number between brackets gives the photometric accuracy. The dotted lines in each panel give the combined 1σ errors. In this figure we have included non-dwarf galaxies that were observed as part of the WHISP program and that will be published in a later paper.

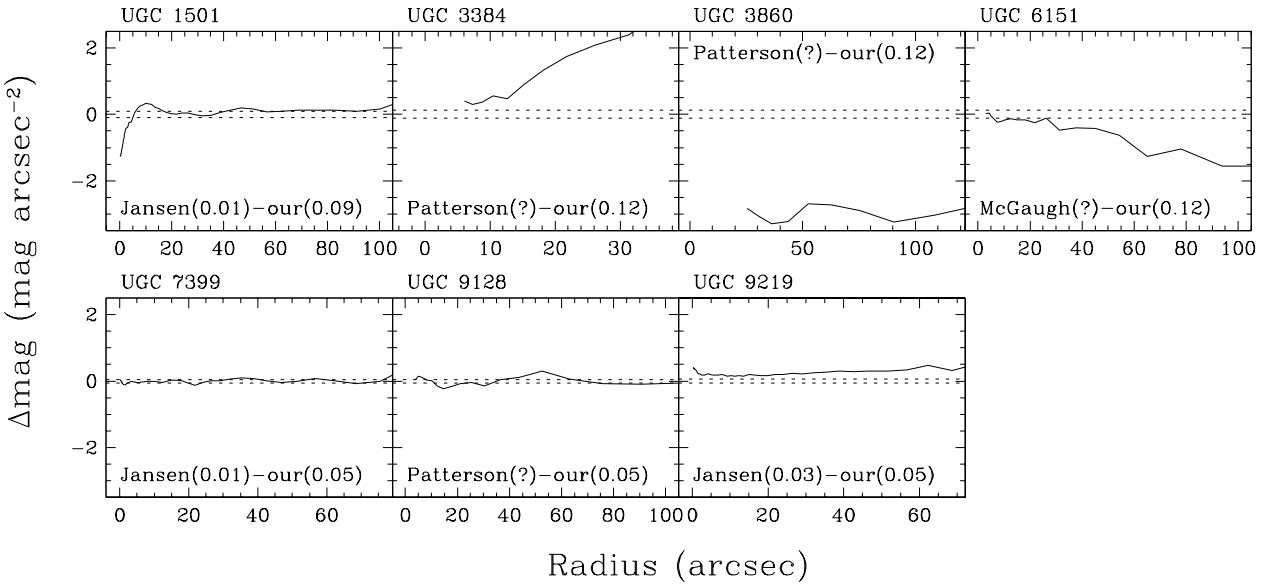

Fig. 7. Same as Figure 6, but for the *B*-band observations.

marked in Tables A.5 and A.6. The fact that the difference profiles in Figs. 4 and 5 are quite flat indicates that, for 80% of the sample, uncertainties due to flatfielding, sky brightness determination and contamination by halos of foreground stars together are below 0.1 mag arcsec^{-2} over the entire radial range.

7.2. External comparison

Comparing surface brightness profiles with those obtained by other authors is not straightforward. For the comparison with published data, we restricted ourselves to CCD data. We have used data by McGaugh & Bothun (1994), de Jong & van de Kruit (1994), Heraudeau & Simien (1996), Patterson & Thuan (1996) and Jansen et al (2000). Where the authors have derived surface brightness profiles with fixed position angle and ellipticity, our profiles were rederived with the same orientation parameters. McGaugh & Bothun (1994) and Patterson & Thuan (1996) used free fits, making comparison of the profiles difficult. To get a substantial sample for comparison with other data, not only the data for the dwarf galaxies were used, but also the data for other galaxies that were observed in this program.

Fig. 6 shows the comparison for the *R*-band profiles. Most profiles are consistent within the 1σ errors, as indicated by the dotted lines. For three galaxies, our results deviate significantly from the profiles obtained by others: UGC 1551, UGC 6446 and UGC 12754. For UGC 1551 there are two independent measurements available in the literature, by Jansen et al (2000) and de Jong & van der Kruit (1994), which are in agreement with each other. The quality of those data for these galaxies is high, as judged by the authors. The three deviating galaxies were observed

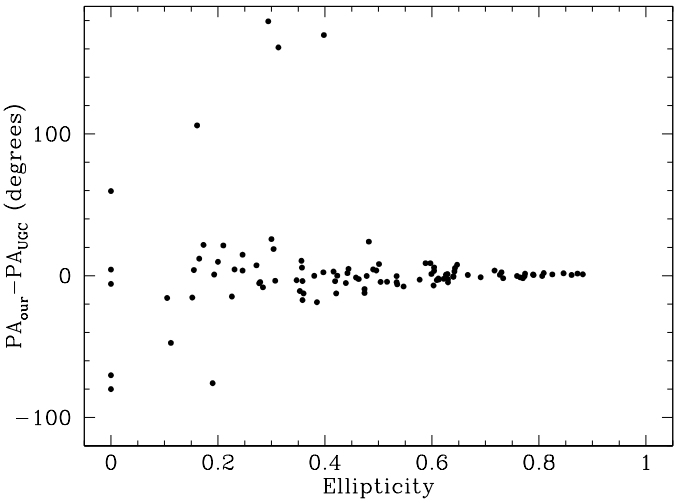

Fig. 8. Comparison of our position angle and the UGC position angle as a function of ellipticity.

during nights that suffered from occasionally thicker cirrus. Based on the external comparison, we conclude that for 87% of our observations the quoted photometric uncertainty is an accurate estimate of the photometric quality, similar to the number found from the internal comparison.

The comparison with the published surface brightness profiles for the *B*-band is presented in Fig. 7. The comparison with the data by Jansen et al (2000) shows that our data is consistent within the uncertainties with his. However, the comparison with the data by McGaugh & Bothun (1994) and Patterson & Thuan (1996) shows clear inconsistencies. Both groups of authors have used free fits rather than fixed fits as we did. This explains the large difference found for UGC 3384, because this galaxy is highly asymmetric. Neither of the authors give uncertainties for

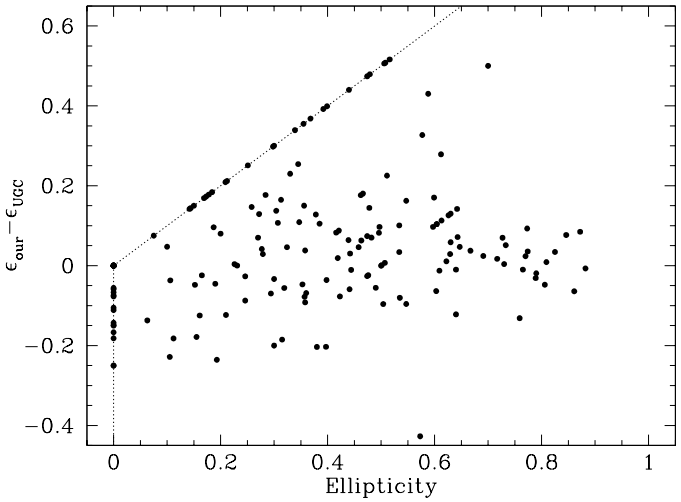

Fig. 9. Comparison of our ellipticity and the UGC ellipticity as a function of our ellipticity. The dotted line corresponds to $\epsilon_{our} = 0$ or $\epsilon_{UGC} = 0$

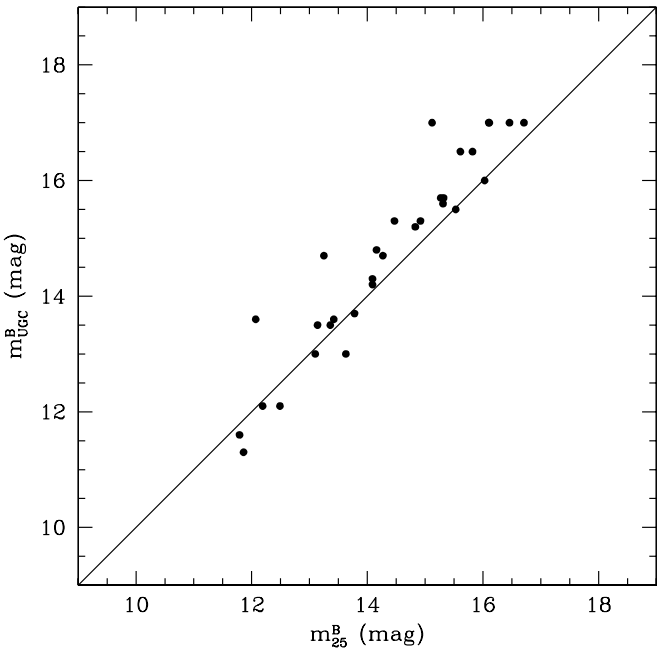

Fig. 10. Comparison of the isophotal B-band magnitude m^B_{25} and the magnitude quoted in the UGC. The solid line is the line of equality.

their data. Except for UGC 3860, the profiles are fairly consistent, in particular in the inner parts.

In conclusion, based on both the internal and external comparison, we find that our quoted photometric uncertainties are accurate estimates of the real photometric uncertainties. In about 13% of the cases the real photometric uncertainties are underestimated. However, these poor nights are overrepresented in this comparison because many of the galaxies observed in non-photometric nights were deliberately reobserved in order to obtain better photometry. It is therefore likely that for a larger fraction than the 87% quoted above the photometric is uncertainty is accurate.

7.3. Comparison to UGC

An additional source to check our data against is the UGC. Fig. 8 shows the differences between our position angle and those listed in the UGC. For highly inclined galaxies the agreement is excellent. Towards more face-on galaxies the scatter increases and some large differences occur. The outcome of this comparison in no doubt affected by the fact that we have determined the position angles at fainter surface brightness levels.

Fig. 9 shows the comparison of our ellipticities with those from the UGC. The UGC ellipticities have been determined from the major and minor-axis diameters listed in the UGC. There is good general agreement, but with a large scatter, as was to be expected because our ellipticities have been determined at fainter surface brightness levels, and because the UGC ellipticities are based on eye estimates.

In Fig. 10 the m^B_{25} is compared with the B-band magnitude given in the UGC catalog. Generally, the agreement is good for $m^B_{25} \lesssim 14.0$. For fainter galaxies, the UGC magnitudes are systematically too faint. This effect was already noted by Thuan & Seitzer (1979). The difference becomes even more pronounced if the UGC magnitudes are compared with the total magnitude $m_{\rm tot}$, where the difference may be as high as two magnitudes.

A comparison of the UGC R-band diameters with the D_{25} diameters as determined from our R-band radial surface brightness profiles shows good agreement, as can be seen in Fig. 11. This indicates that the limiting surface brightness at which the UGC diameter is measured is about 25 R-band mag arcsec^{-2}. A similar comparison of the B-band diameters shows that the limiting surface brightness there is about 26.5 B-band mag arcsec^{-2}, in close agreement with the value of 26.53 found by Fouqué & Paturel (1985).

8. Discussion

As described in Sect. 2, this sample contains a range in galaxy types and properties. Here we briefly characterize the sample by showing the distribution of several parameters.

The distribution of ellipticities ϵ and position angles PA are given in Fig. 12. The ellipticities have been derived as described in Sect. 5. The peak at $\epsilon = 0$ is artificial and occurs because the ellipticities were set to zero for galaxies in which the ellipticities were equal to zero within the uncertainties. The true values of the ellipticities for these galaxies probably spread over a range in ellipticities, up to $\epsilon \sim 0.3$, filling in the depression near $\epsilon = 0.1$. This makes the distribution of ellipticities more or less uniform for small ϵ. Ellipticities near $\epsilon = 1$ are missing because

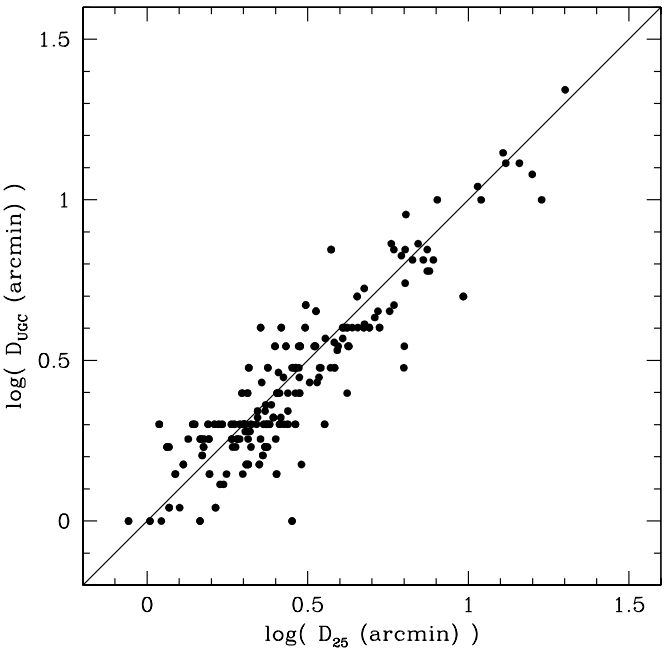

Fig. 11. Comparison of D_{25} with the optical diameter as listed in the UGC for the R-band. The solid line is the line of equality.

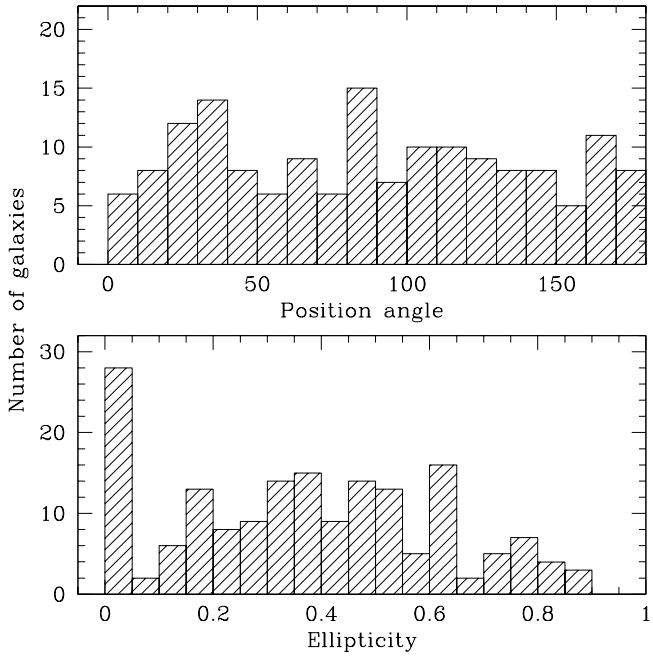

Fig. 12. The distribution of position angle (top panel) and of ellipticities (bottom panel) of the galaxies in our sample.

of the finite thickness of the galaxies. The distribution of position angles is consistent with being flat, as is expected if the galaxy orientations are random.

Fig. 13 shows the distribution over absolute R-band magnitude for the galaxies in our sample. The absolute magnitudes have been calculated from the total magnitude $m_{\rm tot}$ and the distances listed in Table A.1, and range

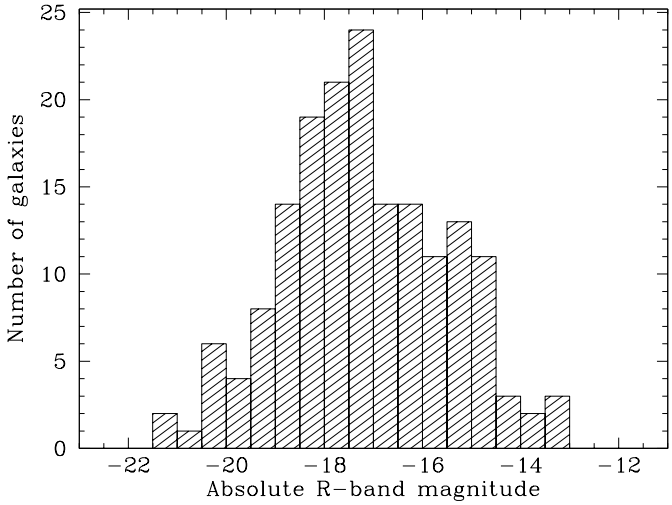

Fig. 13. Histogram of absolute R-band magnitudes for the galaxies in our sample.

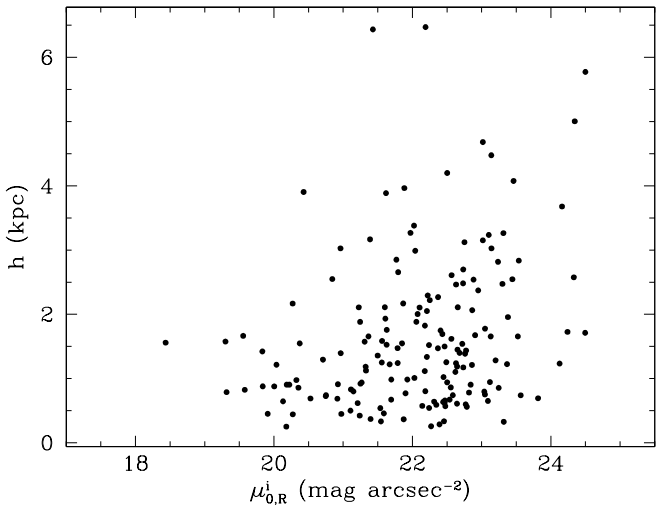

Fig. 14. The scale lengths plotted against the inclination corrected central disk surface brightnesses for the galaxies in our sample.

from $M_R = -22$ to -12. Most of the galaxies in our sample have low luminosities, as expected for dwarf galaxies, but about 30% have $M_R < -18$. These galaxies are not true dwarf galaxies, but form a mixed bag of large low surface brightness galaxies (similar to the galaxies studied by e.g., de Blok et al 1995 and Sprayberry et al 1995) and bright interacting galaxies. These galaxies were included in the sample because our selection is largely based on morphological type.

Fig. 14 shows this point more clearly. In this figure, for each galaxy the inclination corrected central disk surface brightness μ_0^i is plotted against the scale length. About 30% of the galaxies have scale lengths larger than 2 kpc. These are the galaxies that are more typical of the large low surface brightness galaxies. De Blok et al (1995) find

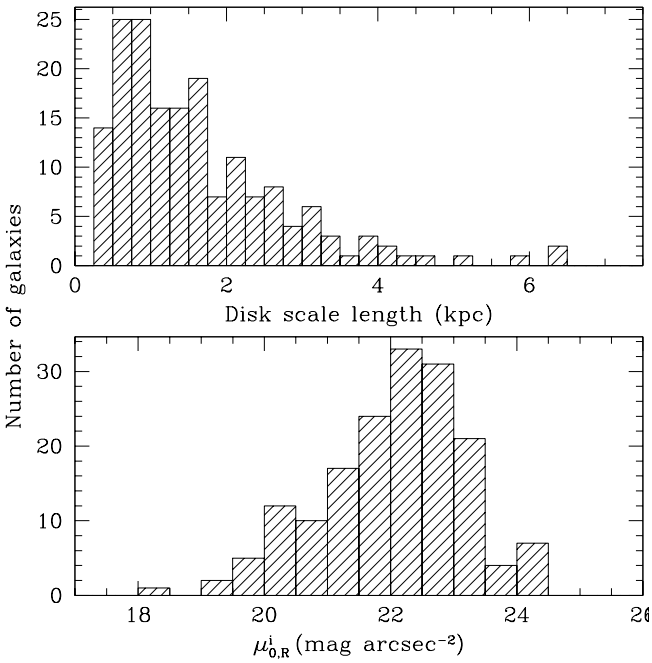

Fig. 15. The distribution of scale lengths (top panel) and of inclination corrected central surface brightnesses for the galaxies in our sample.

that these galaxies typically have scale lengths between 2 and 6 kpc, and surface brightnesses fainter than $\mu_R = 22$ mag arcsec^{-2}. Note that the selection on late type has not included galaxies with both large scale length and high central surface brightness.

Finally, Fig. 15 shows the distribution of scale lengths and of inclination corrected central disk surface brightnesses. The galaxies in our sample generally have small scale lengths. The range in surface brightnesses is large, spanning from $\mu^i_{0,R} = 19$ to 25 mag arcsec^{-2}.

9. Summary

We provide R-band surface photometry for 171 late-type galaxies. We have obtained magnitudes, diameters, central surface brightnesses, extrapolated central surface brightnesses and scale lengths. For all galaxies we have presented elliptically-averaged surface brightness profiles, and profiles showing the run of ellipticity, position angle profiles and isophote center with radius. Flatfielding achieved a median accuracy of 0.22%, making the surface brightness and structural profiles reliable to about 26 R mag arcsec^{-2} in most cases. The zero point uncertainty is less than 0.1 mag for 77% of the sample, and less than 0.2 mag for 89% of the sample. The photometric accuracy is reliably quantified for each galaxy by the 1σ errors in the photometric calibration. Comparison of our surface brightness profiles and photometric zero points with data from other authors shows that, for at least 85% of the sample, we obtain agreement consistent with the quoted photometric uncertainties.

Acknowledgements. We are grateful to Tjeerd van Albada for valuable comments. We thank Rolf Jansen for making available his data before publication. Travel grant support for this work was provided by the E.U. ANTARES Astrophysics Network, under contract CHRX-CT.93.0359, and by the Leids Kerkhoven-Bosscha Fonds. This research has made use of the NASA/IPAC Extragalactic Database (NED) which is operated by the Jet Propulsion Laboratory, California Institute of Technology, under contract with the National Aeronautics and Space Administration. IRAF is distributed by the National Optical Astronomy Observatories, which are operated by the Association of Universities for Research in Astronomy, Inc., under cooperative agreement with the National Science Foundation. The Digitized Sky Survey (DSS) was produced at the Space Telescope Science Institute under U.S. Government grant NAG W-2166.

References

Aparicio, A., García-Pelayo, J. M., & Moles, M. 1988, A&AS, 74, 367
Arp, H. 1966, ApJS, 14, 1
Bell, E. F., & de Jong, R. S. 2000, MNRAS, 312, 497
Bottinelli, L., Gouguenheim, L., Paturel, G., & de Vaucouleurs, G. 1985, ApJS, 59, 293
Burstein, D., & Heiles, C. 1984, ApJS, 54, 33
Conselice, C. J., Bershady, M. A., & Jangren, A. 2000, ApJ, 529, 886
Courteau, S. 1996, ApJS, 103, 363
Courteau, S., de Jong, R. S., & Broeils, A. H. 1996, ApJ, 457, L73
de Blok, W. J. G., van der Hulst, J. M., & Bothun, G. D. 1995, MNRAS, 274, 235
de Grijs, R. 1998, MNRAS, 299, 595
de Grijs, R., & Peletier, R. F. 1997, A&A, 320, L21
de Grijs, R., & van der Kruit, P. C. 1996, A&AS, 117, 19
de Grijs, R., Kregel, M., & Wesson, K. H. 2000, MNRAS, 324, 1074
de Jong, R.S. 1996a, A&A, 313, 45
de Jong, R.S. 1996b, A&A, 313, 377
de Jong, R., & van der Kruit, P. C. 1994, A&AS, 107, 419
de Vaucouleurs, G. 1975, in Galaxies and the Universe, Vol. IX of Stars and Stellar Systems, eds. A. Sandage, M. Sandage, J. Christian (University of Chicago, Chicago), p. 557
de Vaucouleurs, G. 1979, ApJ, 227, 729
de Vaucouleurs, G., de Vaucouleurs, A., & Buta, R. 1983, AJ, 88, 764
de Vaucouleurs, G., de Vaucouleurs, A., Corwin, H. G., et al. 1991, Third Reference Catalogue of Bright Galaxies (New York:Springer)
Fouqué, P., & Paturel, G. 1985, A&A, 150, 192
Franx, M., Illingworth, G., & Heckman, T. 1989, AJ, 98, 538
Frei, Z., Guhathakurta, P., Gunn, J. E., & Tyson, J. A. 1996, AJ, 111, 174
Gallagher, J. S., & Hunter, D. A. 1989, AJ, 98, 806
Georgiev, T. B., Bilkina, B. I., Tikhonov, N. A., & Karachentsev, I. D. 1991, A&AS, 89, 529
Graham, A. W., & Prieto, M. 1999, ApJ, 524, L23
Han, M. 1992, ApJS, 81, 35
Heraudeau, P.,& Simien, F. 1996, A&AS, 118, 111
Hoessel, J. G., Saha, A., Krist, J., & Danielson, G. E. 1994, AJ, 108, 645
Humphreys, R. M. 1983, ApJ, 269, 335

Humphreys, & R. M, Aaronson, M. 1987, ApJ, 318, L69
Israel, F. P. 1988, A&A, 194, 24
Jansen, R. A. 2000, PhD thesis, Rijksuniversiteit Groningen
Jansen, R. A., Franx, M., Fabricant, D., & Caldwell, N. 2000, ApJS, 126, 271
Jørgensen, I., Franx, M., & Kjærgaard, P. 1992, A&AS, 95, 489
Karachentsev, I. D., & Tikhonov, N. A. 1993, A&AS, 100, 227
Karachentsev, I. D., & Tikhonov, N. A. 1994, A&A, 286, 718
Karachentsev, I. D., Musella, I., & Grimaldi, A. 1996, A&A, 310, 722
Karachentsev, I. D., Tikhonov, N. A., & Sazonova, L. N. 1994a, Sov. Astro. J. Lett., 20 84
Karachentsev, I. D., Tikhonov, N. A., & Sazonova, L. N. 1994b, A&AS, 106, 555
Karachentsev, I. D., Tikhonov, N. A., Sharina, M. E., Georgiev, T. B., & Bilkina, B. I. 1991, A&AS, 91, 503
Kornreich, D. A., Haynes, M. P., & Lovelace, R. V. E. 1998, AJ, 116, 2154
Kraan-Korteweg, R. C. 1986, A&AS, 66, 255
Krismer, M, Tully, R. B., & Gioia, I. M. 1995, AJ, 110, 1584
Landolt, A. U. 1992, AJ, 104, 340
Lyo, A.-R., & Lee, M. G. 1997, JKAS, 30, 27
Matthews, L. D. & Gallagher, J. S. 1997, AJ, 114, 1899
McGaugh, S. S., & Bothun, G. D. 1994, AJ, 107, 530
Nilson, P. 1973, Uppsala General Catalogue of Galaxies, Uppsala Astr. Obs. Ann., Vol. 6 (UGC)
Patterson, R. J., & Thuan, T. X. 1996, ApJS, 107, 103
Paturel, G., García, A. M., Fouqué, P, & Buta, R. 1991, A&A, 243, 319
Peletier, R. F., & Balcells, M. 1996, AJ, 111, 2238
Peletier, R. F., & Balcells, M. 1997, NewAst, 1, 349
Pierce, M. J., Ressler, M. E., & Shure, M. S. 1992, ApJ, 390, L45
Pohlen, M., Dettmar, R.-J, & Lütticke, R. 2000, A&A, 357, L1
Rieke, G. H., & Lebofksy, M. J. 1985, ApJ, 288, 618
Rix, H., & Zaritsky, D. 1995, ApJ, 447, 82
Rozanski, R., & Rowan-Robinson, M. 1994, MNRAS, 271, 530
Sackett, P. D., Morrison, H. L., Harding, P., & Boroson, T.A. 1994, Nature, 370, 441
Saha, A., Labhardt, L, Schwengeler, H., et al., 1994, ApJ, 425, 14
Schmidt, K.-H., & Boller, T. 1992, AN, 313, 189
Schmidt, K.-H., & Karachentsev, I. D. 1996, AN, 317, 197
Sersic, J. L., 1968, Atlas de galaxias australes, Observatorio Astronomico, Cordoba
Sharina, M. E. 1991, Sov. Astro. J. Lett., 17, 383
Skillman, E. D., Kennicutt, R. C., & Hodge, P. W. 1989, ApJ, 347, 875
Sprayberry, D., Impey, C. D., Bothun, G. D., & Irwin, M. J. 1995, AJ, 109, 558
Swaters, R. A. 1999, PhD thesis, Rijksuniversiteit Groningen
Swaters, R. A., van Albada, T. S., van der Hulst, J. M., & Sancisi, R. 2000, A&AS, accepted (Paper I)
Thuan, T. X., & Seitzer, P. O. 1979, ApJ, 231, 680
Tikhonov, N. A., Bilkina, B. I., Karachentsev, I. D., & Georgiev, T. B. 1991, A&A, 89, 1
Tikhonov, N. A., Karachentsev, I. D., Bilkina, B. I., & Sharina, M. E. 1992, A&Ap Trans, 1, 269
Tolstoy, E., Saha, A., Hoessel, J. G., & McQuade, K. 1995, AJ, 110, 1640
Tully, R. B. 1980, ApJ, 237, 390
Tully, R. B., Verheijen, M. A. W., Pierce, M. J., Huang, J.-S., & Wainscoat, R. J. 1996, AJ, 112, 2471
van den Bergh, S. 1959, Publ David Dunlop Obs. II, No. 5.
van den Bergh, S., 1966, AJ, 71, 922
van Dokkum, P. G., Peletier, R. F., & de Grijs, R., Balcells, M. 1994, A&A, 286, 415
Veron-Cetty, M. P., & Veron, P. 1996, ApJS, 115, 97
Zaritsky, D., & Rix, H. 1997, ApJ, 477, 118

Appendix A: Tables

A.1. Table A.1 – Global properties

Column (1) gives the UGC number.
Column (2) provides other common names, in this order: NGC, DDO (van den Bergh 1959, 1966), IC, Arp (Arp 1966), CGCG. At most two other names are given.
Columns (3) and (4) give the equatorial coordinates (2000) derived from the optical images, as described in Sect. 4.
Column (5) gives the morphological type according to the RC3, using the same coding.
Column (6) gives the absolute B-band magnitude, calculated from the apparent photographic magnitude as given in the RC3, and the distance as given in column 7.
Column (7) provides the adopted distance. Where possible stellar distance indicators have been used, mostly Cepheids and brightest stars. If these were not available, a distance based on group membership was used. If these were not available either, the distance was calculated from the HI systemic velocity following the prescription given in Kraan-Korteweg (1986), with an adopted Hubble constant of $H_0 = 75$ km s^{-1} Mpc^{-1}. A full list of published distances for the galaxies in this sample, updated to the beginning of 1998, is given in Table A.2. For a discussion of the distance uncertainties, see Sect. 3.
Column (8), (9) and (10) give the heliocentric velocity, the HI line width at the 50% level and the HI mass in units of 10^8 $M_\odot$, respectively, all as given in the RC3.
Column (11) gives the Galactic extinction in the R-band, derived from the A_B value according to Burstein & Heiles (1984) assuming A_B/A_R of 1.77 (Rieke & Lebofsky 1985).

A.2. Table A.2 – Adopted distances

Column (1) gives the UGC number
Column (2) gives the distance as derived from the HI systemic velocity, assuming a Hubble constant $H_0 = 75$ km s^{-1}Mpc^{-1} and following the prescription given in Kraan-Korteweg (1986) to correct for the Virgocentric inflow.
Column (3) gives the distance(s) found in the literature.
Column (4) gives the reference for each distance.
Column (5) gives a brief description of the method used in the original paper to derive the distance.
Column (6) gives the distance we have adopted. The distance uncertainties are discussed in Sect. 3.

A.3. Table A.3 and A.4 – List of observations

Column (1) lists the UGC number.
Column (2) gives the observing date.
Column (3) gives the exposure time.
Column (4) gives an estimate of the seeing, as described in Sect. 4.
Column (5) gives the photometric accuracy $\sigma_{\rm phot}$. This is the residual obtained in the photometric solution, as described in Sect. 4.

A.4. Table A.5 and A.6 – isophotal and photometric parameters

Column (1) lists the UGC number.
Column (2) and (3) give the ellipticity ϵ and the position angle P.A.
Column (4) gives the apparent magnitude m_{25} within the 25 mag arcsec^{-2} isophote.
Column (5) gives the apparent limiting magnitude $m_{\rm lim}$. This is the apparent magnitude within the limiting surface brightness $\mu_{\rm lim}$ given in column (7).
Column (6) gives the extrapolated apparent magnitude $m_{\rm ext}$. The extrapolation is described in Sect. 6.
Column (7) gives the limiting surface brightness $\mu_{\rm lim}$, which corresponds to 3σ above sky. σ is our estimate of the 1σ error in the sky, as described see Sect. 4.
Column (8) gives the central surface brightness μ_c, as determined from the luminosity profile (see Sect. 5). μ_c has been corrected for Galactic foreground extinction, but not for inclination.
Column (9) gives the extrapolated disk central surface brightness μ_0 as obtained from an exponential fit to the surface brightness profile. μ_0 has been corrected for Galactic foreground extinction, but not for inclination.
Column (10) gives the absolute magnitude M_R or M_B. The absolute magnitude has been calculated from $m_{\rm ext}$ and the distance as listed in A.2. These values are corrected for Galactic foreground extinction.
Column (11) gives the uncertainty in the photometry, $\sigma_{\rm phot}$, which is the residual obtained in the photometric solution, as described in Sect. 4. For galaxies with $\sigma_{\rm phot} > 0.25$ mag the photometric parameters are only given to the nearest tenth of a magnitude.
Column (12) gives the scale length h in arcsec, measured along the major axis, as determined from an exponential fit to surface brightness profile.
Column (13) and (14) give the isophotal diameters, d_{25} and $d_{26.5}$ at the 25 and 26.5 mag arcsec^{-2} isophote. These diameters have been corrected for Galactic foreground extinction and are measured along the major axis. The diameters are given in units of arcsec.
Column (15), (16) and (17) give the radii r_{20}, r_{50} and r_{80} within which 20%, 50% and 80% of the light is contained. These radii have been measured along the major axis, and are given in units of arcsec.

— *Notes* —

[a] These galaxies are at very low Galactic latitude and therefore Burstein & Heiles (1984) do not give Galactic foreground extinctions. The galaxies concerned are: UGC 192, UGC 3272 and UGC 3390. For these galaxies the magnitudes and surface brightnesses are not corrected for Galactic extinction.
[b] These galaxies have been observed during nights with occasional thin cirrus clouds. Therefore, in some cases the 1σ photometric error may be an underestimate of the true photometric error, as was found in Sect. 7.

Table A.1. Global properties

UGC	Other names	R.A. (2000) $h\ m\ s$	Dec. (2000) $^\circ\ '\ ''$	Type	M_B	D	$v_{\rm HI}$	W_{50}	$M_{\rm HI}$	A_R
					mag	Mpc	km/s	km/s	10^8 $M_\odot$	mag
(1)	(2)	(3)	(4)	(5)	(6)	(7)	(8)	(9)	(10)	(11)
192	IC 10	0 20 20.0	59 17 56	.IB.9$.	–	1.0	-343	63	1.33	–
731	DDO 9	1 10 43.6	49 36 4	.I..9*.	–	8.0	639	130	5.99	0.41
1249	IC 1727	1 47 29.9	27 19 56	.SBS9..	-17.59	7.5	338	121	8.2	0.14
1281		1 49 31.9	32 35 24	.S..8..	-15.82	5.5	157	116	2.83	0.08
1438	NGC 746	1 57 51.1	44 55 6	.I..9..	-17.11	13.3	712	105	8.38	0.31
1501	NGC 784	2 01 16.9	28 50 10	.SB.8*/	-16.86	5.7	198	96	5.05	0.12
1547	DDO 17	2 03 20.4	22 02 31	.IB.9..	-17.22	20.2	2644	138	25.9	0.15
1551		2 03 37.6	24 04 32	.SB?...	-18.02	20.2	2671	118	14.1	0.19
1865	DDO 19	2 24 59.9	36 02 15	.S..9*.	–	10.1	580	76	3.22	0.12
2014	DDO 22	2 32 54.0	38 40 35	.I..9*.	–	10.1	565	49	1.94	0.1
2017		2 32 45.4	28 50 29	.I..9..	–	16.2	1014	84	9.09	0.16
2023	DDO 25	2 33 18.2	33 29 28	.I..9*.	-15.61	10.1	606	39	4.06	0.19
2034	DDO 24	2 33 43.1	40 31 43	.I..9..	-15.71	10.1	579	45	8.17	0.1
2053	DDO 26	2 34 29.2	29 45 4	.I..9..	-15.35	11.8	1029	59	5.59	0.2
2455	NGC 1156	2 59 42.2	25 14 15	.IBS9..	-17.45	7.8	382	67	10.7	0.37
2603		3 19 14.6	81 20 47	.I..9..	–	38.5	2519	121	43.1	0.39
2800		3 40 03.8	71 24 20	.I..9?.	–	20.6	1176	208	29.3	0.77
3056	NGC 1569, Arp 210	4 30 49.6	64 50 53	.IB.9..	-14.8	2.2	-88	74	1.12	1.15
3060	NGC 1560	4 32 48.3	71 52 50	.SAS7./	-16.15	3.9	-35	125	10.3	0.35
3137		4 46 15.0	76 25 6	.S?....	-16.22	18.4	993	222	35.4	0.31
3144	DDO 33	4 47 54.5	74 55 46	.IB.9..	-16.24	19.5	1636	142	22.8	0.32
3273		5 17 44.9	53 33 1	.S..9..	-15.62	12.2	616	185	19	–
3317	DDO 38	5 33 37.7	73 43 30	.I..9..	–	19.5	1239	107	14.3	0.26
3371	DDO 39	5 56 37.5	75 19 0	.I..9*.	–	12.8	816	129	12.6	0.27
3384		6 01 37.3	73 07 1	.S..9*.	–	19.5	1086	78	17.5	0.3
3390		6 02 05.3	36 06 17	.SX.8..	–	23.2	1517	202	27.2	–
3475		6 30 28.9	39 30 15	.S..9*.	-15.33	9.3	486	167	4.88	0.66
3647	DDO 40	7 04 50.2	56 31 9	.IB.9..	–	18.4	1384	50	10.2	0.08
3698		7 09 18.8	44 22 49	.I..9*.	–	8.5	426	50	1.76	0.23
3711	NGC 2337	7 10 13.6	44 27 27	.IB.9..	-16.71	8.6	434	144	6.86	0.21
3817		7 22 44.6	45 06 31	.I..9*.	–	8.7	438	43	1.88	0.19
3851	NGC 2366, DDO 42	7 28 52.9	69 12 45	.IBS9..	-15.98	3.4	100	96	7.92	0.1
3860	DDO 43	7 28 17.5	40 46 11	.I..9..	-14.05	6.8	354	38	1.3	0.12
3966	DDO 46	7 41 26.1	40 06 39	.I..9..	–	6.0	361	71	1.69	0.12
4173		8 07 10.5	80 07 38	.I..9*.	-15.82	16.8	862	0	20.2	0.06
4274	NGC 2537, Arp 6	8 13 14.7	45 59 24	.SBS9P.	-16.98	6.6	447	96	2.06	0.08
4278	IC 2233	8 13 58.8	45 44 36	.SBS7*/	-16.62	10.5	563	180	13.3	0.08
4305	Arp 268	8 19 07.4	70 43 24	.I..9..	-16.75	3.4	158	66	8.21	0.05
4325	NGC 2552	8 19 19.7	50 00 32	.SAS9$.	-17.42	10.1	519	134	7.52	0.1
4426	DDO 52	8 28 28.3	41 51 22	.I..9*.	–	6.4	393	83	1	0.07
4483		8 37 03.5	69 46 32	.I..9*.	-12.77	3.6	156	49	0.41	0.08
4499		8 37 41.4	51 39 9	.SX.8..	-17.06	13.0	692	126	12	0.07
4543		8 43 21.7	45 44 10	.SA.8..	-18.1	30.3	1960	108	60	0.06
4660		8 54 24.2	34 33 22	.S..9*.	–	32.9	2203	61	18.6	0.03
4704		8 59 00.3	39 12 39	.S..8*.	-15.03	10.2	596	129	5.56	0.03
4945		9 22 25.8	75 46 2	.I..9..	–	6.7	659	34	0.38	0
5040		9 27 36.4	28 47 58	.I..9?.	-19.81	58.0	4149	63	70.2	0
5139	DDO 63	9 40 28.8	71 10 57	.IXS9..	-14.65	6.8	136	26	4.88	0.03
5221	NGC 2976	9 47 14.9	67 55 2	.SA.5P.	-17.3	4.5	3	97	2.57	0.06
5272	DDO 64	9 50 22.7	31 29 14	.I..9..	-14.82	6.1	520	82	1.52	0.02
5322	NGC 3034	9 55 52.7	69 40 52	.I.0../	-19.61	5.9	203	146	18.2	0.07
5336	DDO 66	9 57 31.7	69 02 48	.I..9..	–	3.6	46	69	3.28	0.08
5340	DDO 68	9 56 45.7	28 49 34	.I..9P*	-14.82	6.1	503	78	2.6	0.02
5364	DDO 69	9 59 25.2	30 44 48	.IB.9..	-13.9	2.2	20	33	0.74	0.04
5398	NGC 3077	10 03 19.1	68 44 5	.I.0.P.	-16.98	3.6	14	65	10.5	0.12
5414	NGC 3104, Arp 264	10 03 58.4	40 45 24	.IXS9..	-16.39	10.0	612	100	5.75	0.02
5455		10 08 50.3	70 38 3	.I..9..	–	22.6	1290	57	9.55	0.1

Table A.1. – Continued

UGC	Other names	R.A. (2000) $h\ m\ s$	Dec. (2000) $^\circ\ '\ ''$	Type	M_B	D	$v_{\rm HI}$	W_{50}	$M_{\rm HI}$	A_R
					mag	Mpc	km/s	km/s	10^8 $M_\odot$	mag
(1)	(2)	(3)	(4)	(5)	(6)	(7)	(8)	(9)	(10)	(11)
5478	DDO 73	10 09 31.5	30 09 2	.I..9..	-17.03	18.5	1378	55	5.83	0.03
5612	DDO 77	10 24 07.2	70 52 55	.SBS8..	-16.56	13.6	1011	146	10	0.11
5666	IC 2574	10 28 23.0	68 24 56	.SXS9..	-17.03	3.7	47	115	13.3	0.03
5688	DDO 80	10 30 25.0	70 03 3	.SB.9*.	–	30.2	1921	54	32.7	0
5706		10 31 10.8	34 30 13	.I..9..	–	24.5	1494	36	5.78	0.01
5721	NGC 3274	10 32 17.3	27 40 8	.SX.7?.	-15.95	6.7	537	157	6.85	0.03
5740		10 34 47.0	50 46 11	.SX.9..	-15.27	11.9	651	117	4.52	0
5764	DDO 83	10 36 43.5	31 32 50	.IBS9*.	-15.36	9.0	586	101	2.56	0.02
5829	DDO 84	10 42 43.2	34 27 1	.I..9..	-15.76	9.0	630	75	12.7	0.02
5846	DDO 86	10 44 29.9	60 22 6	.I..9..	-15.69	13.2	1019	44	7.06	0
5860	NGC 3353	10 45 22.4	55 57 37	.S..3$P	-17.93	17.4	944	96	8.25	0
5918	VII Zw 347	10 49 37.0	65 31 48	.I..9*.	–	7.7	338	62	2.45	0
5935	NGC 3396, Arp 270	10 49 55.4	32 59 27	.IB.9P.	-19.49	26.4	1625	160	56.3	0
5986	NGC 3432, Arp 206	10 52 31.3	36 37 9	.SBS9./	-17.92	8.7	616	232	22.8	0
6016		10 54 13.0	54 17 14	.I..9..	–	25.2	1493	136	25	0
6021	NGC 3445	10 54 35.6	56 59 27	.SXS9..	-19.66	32.1	2023	102	43.3	0
6024	NGC 3448	10 54 38.9	54 18 21	.I.0...	-19.78	23.2	1350	239	79.9	0
6126	NGC 3510	11 03 43.4	28 53 11	.SBS9./	-16.75	8.9	705	186	9.17	0
6151	DDO 91	11 05 56.4	19 49 35	.S..9*.	-16.87	17.2	1331	26	4.39	0
6161		11 06 49.2	43 43 23	.SB.8..	-16.54	12.9	758	108	9.57	0
6251	DDO 92	11 13 26.8	53 35 44	.SX.9*.	-15.59	13.2	927	44	4.79	0
6406	NGC 3657	11 23 55.6	52 55 16	.SXT5P.	-18.53	21.5	1215	196	39.1	0
6446		11 26 40.4	53 44 50	.SA.7..	-16.59	12.0	645	135	14.1	0
6456	VII Zw 403	11 27 58.7	78 59 38	.P.....	-12.88	3.0	-92	49	0.33	0.05
6565	NGC 3738, Arp 234	11 35 48.6	54 31 28	.I..9..	-15.71	3.2	229	78	0.73	0
6628		11 40 05.8	45 56 32	.SA.9..	-17.01	15.3	850	40	13.3	0.01
6682	DDO 96	11 43 09.0	59 06 24	.S..9*.	–	16.1	1326	73	7.33	0
6817	DDO 99	11 50 54.1	38 52 54	.I..9..	-13.71	4.02	245	37	1.49	0
6840	DDO 100	11 52 07.0	52 06 29	.SBT9..	-15.77	15.7	1046	143	8.86	0.01
6912	VII Zw 430	11 56 13.9	58 11 60	.S?....	-17.26	23.6	1357	96	22.1	0
6917		11 56 28.7	50 25 42	.SB.9..	-17.63	16.9	910	183	19.3	0.02
6944	NGC 3995, Arp 313	11 57 44.1	32 17 38	.SA.9P.	-20.52	47.4	3254	133	148	0.01
6955	DDO 105	11 58 29.1	38 04 33	.IBS9*.	-16.11	11.6	909	144	10.5	0
6956	DDO 102	11 58 26.1	50 55 6	.SBS9..	–	15.7	917	52	6.3	0.02
6995	NGC 4032	12 00 32.9	20 04 25	.I..9*.	-19.08	22.6	1269	103	22.4	0.03
7047	NGC 4068	12 04 02.2	52 35 25	.IA.9..	-14.71	3.5	211	51	1.04	0
7125		12 08 42.1	36 48 10	.S..9..	-17.24	19.5	1071	132	46.9	0.01
7151	NGC 4144	12 09 58.2	46 27 28	.SXS6$/	-15.58	3.5	267	150	1.58	0
7199	NGC 4163	12 12 09.0	36 10 6	.IA.9..	-14.25	3.5	164	30	0.24	0
7204	NGC 4173	12 12 21.2	29 12 29	.SB.7*.	-18.33	20.3	1104	117	40	0.01
7232	NGC 4190	12 13 44.6	36 38 9	.I..9P.	-14.47	3.5	230	46	0.59	0
7261	NGC 4204	12 15 14.2	20 39 34	.SBS8..	-16.89	9.1	861	85	6.63	0.04
7278	NGC 4214	12 15 39.2	36 19 37	.IXS9..	-17.53	3.5	291	62	8.09	0
7306	NGC 4236	12 16 42.8	69 27 46	.SBS8..	-17.05	3.0	0	162	13	0.03
7323	NGC 4242	12 17 30.1	45 37 10	.SXS8..	-18.02	8.1	517	115	7.06	0
7356		12 19 09.1	47 05 25	.I..9?.	–	3.5	272	86	1.15	0
7399	NGC 4288, DDO 119	12 20 38.1	46 17 31	.SBS8..	-16.25	8.4	535	173	6.37	0
7408	DDO 120	12 21 15.4	45 48 47	.IA.9..	-15.31	8.4	462	26	1.63	0
7490	DDO 122	12 24 25.0	70 20 2	.SA.9..	-15.84	8.5	467	69	2.85	0
7524	NGC 4395	12 25 48.8	33 32 50	.SAS9*.	-17.01	3.5	320	109	9.54	0.01
7534	DDO 123	12 26 08.1	58 19 20	.IB.9..	-15.14	8.5	723	55	5.13	0
7559	DDO 126	12 27 05.5	37 08 34	.IB.9..	-12.82	3.2	218	59	0.61	0
7577	DDO 125	12 27 42.0	43 29 37	.I..9..	-13.81	3.5	196	28	0.71	0
7592	NGC 4449	12 28 11.3	44 05 36	.IB.9..	-17.61	3.5	201	136	12.4	0
7599	DDO 127	12 28 27.9	37 14 2	.S..9..	-12.71	3.5	278	66	0.31	0
7603	NGC 4455	12 28 44.1	22 49 18	.SBS7?/	-16.06	6.8	644	132	3.64	0.03
7608	DDO 129	12 28 44.8	43 13 33	.I..9..	–	8.4	538	60	4.88	0

Table A.1. – Continued

UGC	Other names	R.A. (2000) h m s	Dec. (2000) ° ′ ″	Type	M_B mag	D Mpc	$v_{\rm HI}$ km/s	W_{50} km/s	$M_{\rm HI}$ 10^8 $M_\odot$	A_R mag
(1)	(2)	(3)	(4)	(5)	(6)	(7)	(8)	(9)	(10)	(11)
7648	NGC 4485, Arp 269	12 30 31.4	41 42 0	.IBS9P.	-16.74	7.1	493	139	3.48	0
7651	NGC 4490	12 30 36.3	41 38 36	.IBS9P.	-19.29	8.4	578	173	52.9	0
7673	DDO 131	12 31 58.7	29 42 34	.I..9..	–	8.4	642	55	1.56	0.02
7690		12 32 26.9	42 42 17	.I..9*.	-15.99	7.9	537	88	3.07	0
7698	DDO 133	12 32 54.5	31 32 21	.I..9..	-14.71	3.5	333	53	1.2	0.02
7723	NGC 4534	12 34 05.4	35 31 7	.SAS8*.	-17.36	11.3	802	123	19.4	0
7831	NGC 4605	12 40 00.6	61 36 31	.SBS5P.	-17.64	5.2	143	133	3.69	0
7853	NGC 4618, Arp 23	12 41 32.5	41 09 2	.SBT9..	-18.11	7.8	543	97	12.3	0
7861	NGC 4625, IC 3675	12 41 52.5	41 16 20	.SXT9P.	-16.91	9.0	611	66	5.86	0
7866	IC 3687	12 42 15.0	38 30 13	.IXS9..	-13.9	4.8	359	46	1.16	0
7872		12 41 54.1	75 18 27	.I..9..	–	30.7	1887	69	18.6	0.02
7907	NGC 4656	12 43 58.3	32 10 18	.SBS9P.	-18.93	7.9	640	139	49.5	0
7916	I Zw 42	12 44 25.0	34 23 13	.I..9..	–	8.4	607	57	3.6	0.01
7949	DDO 147	12 47 00.1	36 28 41	.I..9*.	–	4.8	333	30	1	0.02
7971	NGC 4707, DDO 150	12 48 22.5	51 09 55	.S..9*.	-15.11	8.4	467	64	2.49	0.01
8005	NGC 4747	12 51 46.0	25 46 35	.SB6$/P	-18.91	21.8	1188	127	31	0.02
8024	NGC 4789A, DDO 154	12 54 05.4	27 08 56	.IBS9..	-14.9	4.8	376	85	4.47	0.01
8098	NGC 4861, IC 3961	12 59 02.0	34 51 41	.SBS9*.	–	12.8	846	86	16.6	0
8188	IC 4182	13 05 49.5	37 36 24	.SAS9..	-15.35	4.7	321	40	3.25	0
8201	VII Zw 499	13 06 25.6	67 42 19	.I..9..	-14.84	4.9	37	44	1.66	0.02
8286	NGC 5023	13 12 11.9	44 02 16	.S..6*/	-15.43	4.8	407	179	3.24	0
8303		13 13 17.6	36 12 58	.IXS9..	-17.07	17.2	946	89	9.97	0
8320	IC 859	13 14 26.4	45 55 34	.IB.9..	-15.35	5.9	195	60	5.93	0
8331	DDO 169	13 15 30.1	47 29 60	.IA.9..	-13.95	5.9	260	50	1.21	0
8441	DDO 175	13 25 29.1	57 49 20	.I..9..	-16.7	20.0	1519	103	15	0
8489	DDO 176	13 29 38.8	45 23 17	.SX.8..	-16.7	20.0	1303	130	12.5	0
8490	NGC 5204	13 29 36.4	58 25 12	.SAS9..	-16.8	4.9	204	110	5.97	0.01
8508	I Zw 60	13 30 44.5	54 54 39	.IA.9..	-13.43	3.7	62	49	0.5	0
8550	NGC 5229	13 34 03.0	47 54 53	.SBS7?/	-14.31	5.3	364	127	1.79	0
8565	NGC 5238, I Zw 64	13 34 42.8	51 36 52	.SXS8..	-14.67	5.2	232	36	0.42	0
8651	DDO 181	13 39 53.9	40 44 21	.I..9..	-14.15	5.9	203	41	1.06	0
8683	DDO 182	13 42 33.1	39 39 28	.I..9..	-15.29	12.6	661	35	2.68	0
8760	DDO 183	13 50 50.5	38 01 5	.I..9..	-13.95	5.9	193	32	0.83	0
8837	DDO 185	13 54 45.8	53 54 10	.IBS9./	-14.83	5.1	144	77	1.24	0
8892		13 57 41.1	57 00 6	.I..9..	-17.3	29.0	1748	95	24	0
9018	NGC 5477, DDO 186	14 05 32.6	54 27 39	.SAS9..	-15.22	7.7	304	52	1.84	0
9128	DDO 187	14 15 56.7	23 03 18	.I..9..	-13.91	4.4	154	33	0.58	0
9211	DDO 189	14 22 32.3	45 22 60	.I..9*.	-15.49	12.6	690	99	9.21	0
9219	NGC 5608	14 23 17.6	41 46 31	.I..9*.	-16.49	12.0	663	109	4.19	0
9240	I Zw 87	14 24 43.6	44 31 37	.IA.9..	-14.66	4.5	153	45	1.14	0
9405	DDO 194	14 35 24.2	57 15 19	.I..9..	–	7.6	222	85	1.38	0
9426		14 37 29.1	48 37 26	.I..9..	–	36.2	2311	44	14.2	0.08
9769		15 12 07.2	55 47 6	.SXT8*.	-16.29	16.6	844	129	14.7	0.01
9906	NGC 5963	15 33 27.8	56 33 36	.S...P.	-17.97	13.7	656	214	20.7	0
9992		15 41 48.0	67 15 15	.I..9..	-14.88	10.4	427	48	2.62	0.05
10736		17 08 04.6	69 27 53	.SX.8..	-15.83	11.7	490	144	7.31	0.1
10792		17 14 02.3	75 12 13	.I..9..	–	22.2	1233	62	9.13	0.09
10806		17 18 51.1	49 53 2	.SBS8..	-17.5	17.7	930	152	16.7	0.04
11283	IC 1291	18 33 52.6	49 16 44	.SBS8?.	-18.57	31.3	1962	173	48.1	0.15
11557		20 24 00.7	60 11 41	.SXS8..	-18.17	23.8	1389	87	26.5	0.65
11707		21 14 31.7	26 44 5	.SA.8..	-16.5	15.9	906	185	34.2	0.36
12048	NGC 7292	22 28 25.8	30 17 34	.IB.9..	-18.18	16.8	986	77	13.3	0.14
12060		22 30 33.9	33 49 14	.IB.9..	-16.07	15.7	884	113	14.9	0.2
12212		22 50 30.2	29 08 20	.S..9*.	–	15.5	894	105	8.88	0.14
12554	NGC 7640	23 22 06.7	40 50 43	.SBS5..	-18.35	9.2	369	234	65.9	0.24
12632	DDO 217	23 29 58.8	40 59 27	.S..9*.	-14.69	6.9	422	114	8.19	0.28
12732		23 40 39.8	26 14 11	.S..9*.	-16.79	13.2	748	112	28.1	0.1

Table A.2. Adopted distances

UGC	D_{HI} (Mpc)	D_{ref} (Mpc)	references	method	D_a (Mpc)
192	0	0.84	KT94	M31 group	
		1.01	KT93	Brightest stars (ph)	
		0.95	SB	Local group	1.0
731	12.75	7.98	dVdVB	NGC 278 group	8.0
1249	7.54				7.5
1281	5.45	5.06	SB	Field	5.5
1438	13.34				13.3
1501	5.74	5.3	SB	Field	5.7
1547	36.99	20.23	dVdVB	NGC 772 group	20.2
1551	37.48				20.2
1865	11.04	7.14	dVdVB	G7 (NGC 1023)	
		10.05	T	TF of NGC 1023 group	10.1
2014	10.97	7.14	dVdVB	G7 (NGC 1023)	
		10.05	T	TF of NGC 1023 group	10.1
2017	16.2				16.2
2023	11.21	7.14	dVdVB	G7 (NGC 1023)	
		10.05	T	TF of NGC 1023 group	10.1
2034	11.26	7.14	dVdVB	G7 (NGC 1023)	
		10.05	T	TF of NGC 1023 group	10.1
2053	16.45	11.75	dVdVB	NGC 972 group	11.8
2455	7.7	7.8	KMG	Brightest stars (CCD)	
		7.07	SB	Field	7.8
2603	38.54				38.5
2800	20.59				20.6
3056	2.24	2.01	KT94	Pair with UGCA 92	
		2.19	I	–	
		3.6	KTG	TF IC342/Maffei group	
		1.85	KTS94a	Brightest stars (CCD)	
		3.56	SB	B1	2.2
3060	3.25	3.88	KTGBS	Brightest stars (ph)	
		3.56	SB	B1	3.9
3137	18.35				18.4
3144	26.79	19.5	dVdVB	IC 391 group	19.5
3273	12.15				12.2
3317	21.55	19.5	dVdVB	IC 391 group	19.5
3371	15.91	12.76	dVdVB	NGC 2146 group	12.8
3384	19.5				19.5
3390	23.2				23.2
3475	9.27				9.3
3647	22.82	18.37	dVdVB	NGC 2549 group	18.4
3698	8.49	8.2	SB	Field	8.5
3711	8.62	8.32	SB	Field	8.6
3817	8.66	8.39	SB	Field	8.7
3851	4.64	2.75	dVdVB	NGC 2403 group	
		3.19	KT94	NGC 2403 group	
		3.44	TSHM	Cepheids	
		3.37	TBKG	Brightest stars (ph)	
		3.31	SB	B2	3.4
3860	6.93	4.57	dVdVB	Group of 3 dwarfs	
		6.76	cited in SK		
		6.6	SB	Field	6.8
3966	6.89	4.57	dVdVB	Group of 3 dwarfs	
		5.97	cited in SK		
		6.58	SB	Field	6.0
4173	16.76				16.8
4274	8.56	6.64	cited in SK		
		8.26	SB	Field	6.6
4278	10.49				10.5
4305	5.51	2.75	dVdVB	NGC 2403 group	
		3.61	KT94	Pair with UGC 4483	
		3.35	TKBS	Brightest stars (ph)	
		3.31	SB	B2	3.4
4325	10.06				10.1
4426	7.15	4.57	dVdVB	Group of 3 dwarfs	
		6.85	SB	Field	
		6.37		Mean: UGC 3860/3977	6.4
4483	5.35	3.61	KT94	Pair with UGC 4305	
		3.63			
		3.31	SB	B2	3.3
4499	12.96				13.0
4543	30.25				30.3
4660	32.89				32.9
4704	10.21				10.2
4945	13.76	6.73			6.7
5040	58.02				58.0
5139	4.94	3.16	dVdVB	G2 (M81)	
		6.78	TKBS	Brightest stars (ph)	
		3.31	SB	B2	6.8
5221	2.46	3.4	KT94	G2 (M81)	
		4.51	KTGBS	Brightest stars (ph)	
		3.31	SB	B2	4.5
5272	7.31	6.14	dVdVB	NGC 2903 group	
		6.85	SB	Field	6.1
5322	5.91				5.9
5336	3.22	3.16	dVdVB	G2 (M81)	
		3.4	KT94	G2 (M81)	
		3.62	GTKB	Brightest stars (ph)	
		3.31	SB	B2	3.6
5340	6.64	6.14	dVdVB	NGC 2903 group	
		6.2	SB	Field	6.1
5364	0	1.1	dVdVB		
		2.23	HSKD	Cepheids	
		1.16	SB	Local group	2.2
5398	2.67	3.56	S	Associated with Garland	
		3.31	SB	B2	3.6
5414	9.99				10.0
5455	22.58				22.6
5478	22.47	18.54	dVdVB	G42 (NGC 2964)	18.5
5612	18.79	13.55	dVdVB	NGC 2985 group	
		6.92	BGPdV	Sosie galaxies	13.6
5666	3.13	3.16	dVdVB	G2 (M81)	
		3.4	KT94	G2 (M81)	
		3.71	TBKG	Brightest stars (ph)	
		3.31	SB	B2	3.7
5688	30.93	30.2	dVdVB	NGC 3329 group	30.2
5706	24.48				24.5
5721	6.56	6.73	cited in SK		
		6.05	SB	Field	6.7
5740	11.86				11.9
5764	7.73	8.95	dVdVB	G12 (NGC 3184)	9.0
5829	8.81	8.95	dVdVB	G12 (NGC 3184)	9.0
5846	18.69	13.18	dVdVB	G28 (NGC 3310)	13.2
5860	17.41				17.4
5918	6.7	3.16	dVdVB	G2 (M81)	
		7.74	SB	B2a	7.7
5935	26.35				26.4
5986	8.74				8.7
6016	25.16				25.2
6021	32.12				32.1
6024	23.24				23.2
6126	8.9				8.9
6151	22.26	17.22	dVdVB	Leo II Cloud	17.2
6161	12.93				12.9
6251	17.14	13.18	dVdVB	G28 (NGC 3310)	13.2
6406	21.5				21.5
6446	12.01				12.0
6456	1.71	3.4	KT94	G2 (M81)	
		3.03	KTS94b	Brightest stars (CCD)	
		1.76	SB	Field	3.0
6565	4.57	3.21	cited in SK		
		3.45	SB	B4	3.2
6628	15.3				15.3
6682	23.19	16.07	dVdVB	NGC 4036 group	16.1
6713	16.52				16.5
6817	3.25	4.02	cited in SK		
		3.45	SB	B4	4.0
6840	19.13	15.7	dVdVB	G34 (NGC 3992)	15.7
6912	23.64				23.6
6917	16.86				16.9
6944	47.43				47.4
6955	15.81	11.59	dVdVB	G17 (NGC 4151)	11.6
6956	17.02	15.7	dVdVB	G34 (NGC 3992)	15.7
6995	22.62				22.6

UGC	D_{HI} (Mpc)	D_{ref} (Mpc)	references	method	D_a (Mpc)
7047	4.11	3.45	SB	B4	3.5
7125	19.47				19.5
7151	4.29	3.45	SB	B4	3.5
7199	2.02	3.45	SB	B4	3.5
7204	20.32				20.3
7232	2.9	3.45	SB	B4	3.5
7261	9.09				9.1
7278	3.66	3.45	SB	B4	3.5
7306	2.49	3.4	KT94	G2 (M81)	
		2.03	BGPdV	Sosie galaxies	
		3.01	TBKG	Brightest stars (ph)	
		3.31	SB	B2	3.0
7323	8.05	6.08	BGPdV	Sosie galaxies	8.1
7356	4.45	3.45	SB	B4	3.5
7399	8.49	8.39	dVdVB	G10 (NGC 4631)	8.4
7408	7.17	8.39	dVdVB	G10 (NGC 4631)	8.4
7490	10.54	8.47	dVdVB	Close to G10	8.5
7524	3.81	3.45	SB	B4	3.5
7534	14.12	8.47	dVdVB	Close to CVn II	8.5
7559	2.83	5.06	dVdVB	G3 (NGC 4736)	
		3.16	cited in SK		
		3.45	SB	B4	3.2
7577	3.08	5.06	dVdVB	G3 (NGC 4736)	
		3.45	SB	B4	3.5
7592	3.2	3.45	SB	B4	3.5
7599	3.6	5.06	dVdVB	G3 (NGC 4736)	
		3.45	SB	B4	3.5
7603	6.8				6.8
7608	8.03	8.39	dVdVB	G10 (NGC 4631)	8.4
7648	7.08				7.1
7651	8.43				8.4
7673	7.53	8.39	dVdVB	G10 (NGC 4631)	8.4
7690	7.94				7.9
7698	3.83	5.06	dVdVB	G3 (NGC 4736)	
		3.45	SB	B4	3.5
7723	11.32				11.3
7831	4.08	4.63	KT94	Near M81 and M101	
		5.18	cited in SK		
		4.16	SB	Field	5.2
7853	7.83				7.8
7861	9				9.0
7866	4.84	5.06	dVdVB	G3 (NGC 4736)	
		4.8	SB	B5	4.8
7872	30.73				30.7
7907	7.9				7.9
7916	7.76	8.39	dVdVB	G10 (NGC 4631)	8.4
7949	4.32	5.06	dVdVB	G3 (NGC 4736)	
		4.8	SB	B5	4.8
7971	8.23	8.39	dVdVB	G10 (NGC 4631)	8.4
8005	21.81				21.8
8024	4.11	5.06	dVdVB	G3 (NGC 4736)	
		4.8	SB	B5	4.8
8098	12.82				12.8
8188	4.38	4.7	SLSMPST	Cepheids	
		2.51	PRS	Brightest stars (CCD)	
		4.8	SB	B5	4.7
8201	3.04	2.41	dVdVB	NGC 4236 group	
		4.63	KT94	Near M81 and M101	
		4.9	KTGBS	Brightest stars (ph)	
		3.31	SB	B2	4.9
8286	6.35	4.8	SB	B5	4.8
8303	17.2				17.2
8320	3.49	5.86	dVdVB	UMa	
		3.55	SB	Field	5.9
8331	4.58	5.86	dVdVB	UMa	
		4.59	SB	Field	5.9
8441	25.99	20.04	dVdVB	NGC 5301 group	20.0
8489	23.06	20.04	dVdVB	NGC 5301 group	20.0
8490	4.95	5.01	BGPdV	Sosie galaxies	
		4.92	cited in SK		
		5.29	SB	B3	4.9
8508	2.46	3.68	cited in SK		
		5.29	SB	B3	3.7
8550	6.37	5.29	SB	B3	5.3
8565	4.72	6.31	KT94	G5 (M101)	
		5.18	cited in SK		
		5.29	SB	B3	5.2
8651	3.33	5.86	dVdVB	UMa	
		3.42	SB	Field	5.9
8683	10.57	12.59	dVdVB	NGC 5033 group	12.6
8760	3.06	5.86	dVdVB	UMa	
		3.2	SB	Field	5.9
8837	3.74	5.11	dVdVB	G5 (M101)	
		5.29	SB	B3	5.1
8892	29.01				29.0
9018	6.46	5.11	dVdVB	G5 (M101)	
		7.73	cited in SK		
		5.29	SB	B3	7.7
9128	1.74	4.37	AGM	Brightest stars (CCD)	
		2.01	SB	Field	4.4
9211	12.98	12.59	dVdVB	NGC 5033 group	12.6
9219	11.95				12.0
9240	3.34	5.86	dVdVB	UMa	
		4.53	cited in SK		
		3.55	SB	Field	4.5
9405	5.64	5.11	dVdVB	G5 (M101)	
		5.29	SB	B3	
		7.62	cited in SK		7.6
9426	36.18				36.2
9769	16.57	16.14	BGPdV	Sosie galaxies	16.6
9906	13.69				13.7
9992	10.38				10.4
10310	14.39	15.56	dVdVB	NGC 6207 group	15.6
10736	11.71				11.7
10792	22.16				22.2
10806	17.73				17.7
11283	31.25				31.3
11557	23.77				23.8
11707	15.9				15.9
11861	25.1				25.1
12048	16.83				16.8
12060	15.69				15.7
12082	14.6	12.53	dVdVB	NGC 7331 group	14.6
12212	15.48				15.5
12554	9.15				9.2
12632	9.83	6.89	dVdVB	NGC 7640 group	6.9
12732	13.23				13.2

AGM	Aparicio, García-Pelayo & Moles 1988
BGPdV	Bottinelli et al. 1985
GTKB	Georgiev et al. 1991
HSKD	Hoessel et al. 1994
I	Israel 1988
KMG	Karachentsev, Musella & Grimaldi 1996
KT93	Karachentsev & Tikhonov 1993
KT94	Karachentsev & Tikhonov 1994
KTGBS	Karachentsev et al. 1991
KTG	Krismer, Tully & Gioia 1995
KTS94a	Karachentsev, Tikhonov & Sazonova 1994a
KTS94b	Karachentsev, Tikhonov & Sazonova 1994b
PRS	Pierce, Ressler & Shure 1992
SB	Schmidt & Boller 1992
SK	Schmidt & Karachentsev 1996
SLSMPST	Saha et al. 1994
S	Sharina 1991
TBKG	Tikhonov et al. 1991
TKBS	Tikhonov et al. 1992
TSHM	Tolstoy et al. 1995
T	Tully 1980
dVdVB	De Vaucouleurs, de Vaucouleurs & Buta 1983

Table A.3. List of R-band observations

UGC	date	$t_{\rm exp}$ sec	seeing $''$	$\sigma_{\rm phot}$ mag
(1)	(2)	(3)	(4)	(5)
192	1994 Nov 29	60	2.2	0.05
731	1995 Dec 23	600	1.0	0.02
1249	1994 Dec 2	600	1.6	0.22
1281	1995 Dec 24	300	0.9	0.02
1438	1994 Dec 2	600	1.1	0.22
1501	1995 Dec 24	300	1.0	0.02
1547	1994 Nov 29	300	1.8	0.05
1551	1994 Nov 29	600	1.8	0.05
1865	1995 Dec 25	600	1.6	0.02
2014	1994 Dec 2	1200	1.5	0.22
2017	1995 Dec 25	1800	1.5	0.05
2023	1995 Dec 25	600	1.6	0.02
2034	1995 Dec 25	600	1.5	0.05
2053	1994 Nov 29	420	3.2	0.05
2455	1994 Nov 29	180	2.5	0.05
2603	1995 Dec 27	900	1.6	0.19
2800	1995 Dec 23	600	1.0	0.02
3056	1994 Dec 3	420	1.3	0.22
3060	1995 Dec 24	600	1.3	0.07
3137	1995 Feb 4	1200	1.6	0.51
3144	1995 Dec 23	600	1.1	0.02
3273	1995 Feb 4	600	1.6	0.51
3317	1995 Dec 24	600	1.2	0.02
3371	1995 Dec 24	900	1.4	0.07
3384	1995 Dec 26	900	1.6	0.19
3390	1995 Dec 26	480	1.6	0.19
3475	1995 Dec 27	900	0.9	0.05
3647	1995 Dec 26	900	1.6	0.19
3698	1995 Dec 27	900	1.1	0.19
3711	1994 May 2	120	1.9	0.01
3817	1994 Dec 3	1200	2.2	0.22
3851	1995 Dec 28	300	2.6	0.02
3860	1995 Dec 26	600	1.5	0.19
3966	1995 Dec 24	600	1.7	0.02
4173	1995 Dec 24	600	1.4	0.02
4274	1995 Dec 26	300	1.4	0.19
4278	1994 Dec 4	180	2.0	0.02
4305	1995 Dec 28	180	1.7	0.01
4325	1995 Dec 24	300	1.7	0.02
4426	1994 Dec 3	1800	1.6	0.22
4483	1995 Dec 26	900	2.3	0.19
4499	1994 Dec 4	300	2.1	0.02
4543	1994 Nov 30	360	2.3	0.05
4660	1995 Dec 24	600	1.9	0.02
4704	1995 Dec 27	600	1.3	0.02
4945	1995 Dec 24	600	1.3	0.02
5040	1995 Dec 26	600	1.7	0.05
5139	1994 May 5	600	1.8	0.01
5221	1994 May 1	300	2.3	0.02
5272	1994 May 4	780	2.1	0.01
5322	1995 Dec 27	300	1.4	0.19
5336	1995 Dec 24	600	1.2	0.02
5340	1994 May 2	1200	1.9	0.01
5364	1994 May 4	1320	2.4	0.01
5398	1994 May 3	360	1.7	0.01
5414	1994 May 1	1320	2.4	0.02
5455	1994 Nov 30	1200	3.4	0.05

Table A.3. – Continued

UGC	date	$t_{\rm exp}$ sec	seeing $''$	$\sigma_{\rm phot}$ mag
(1)	(2)	(3)	(4)	(5)
5478	1995 Dec 25	600	1.7	0.07
5612	1995 Feb 7	600	1.4	0.51
5666	1995 Dec 28	360	1.8	0.19
5688	1994 May 6	600	2.2	0.06
5706	1995 Dec 25	900	1.7	0.07
5721	1994 May 1	600	1.9	0.02
5740	1995 Feb 5	600	1.3	0.51
5764	1995 Feb 5	600	1.4	0.51
5829	1994 May 5	1200	2.3	0.01
5846	1994 May 1	600	1.8	0.02
5860	1995 Dec 27	360	1.2	0.19
5918	1994 May 5	1200	2.4	0.01
5935	1994 May 6	300	1.8	0.06
5986	1994 May 2	300	1.8	0.02
6016	1995 Feb 7	900	1.5	0.51
6021	1995 Dec 27	300	1.2	0.19
6024	1994 May 3	240	2.2	0.01
6126	1994 May 6	300	1.9	0.06
6151	1995 Dec 26	600	1.6	0.19
6161	1994 May 6	1200	1.6	0.06
6251	1995 Dec 28	600	1.5	0.19
6406	1994 Dec 4	300	2.7	0.02
6446	1994 Dec 4	1200	2.7	0.02
6456	1995 Dec 27	600	1.3	0.19
6565	1994 May 3	250	2.3	0.01
6628	1994 May 5	600	2.7	0.01
6682	1995 Dec 27	600	1.3	0.19
6817	1994 May 3	600	1.7	0.01
6840	1994 Dec 4	600	2.3	0.02
6912	1995 Feb 3	600	1.8	0.51
6917	1995 Feb 3	300	2.1	0.51
6944	1994 May 2	240	2.2	0.02
6955	1994 May 3	600	1.8	0.01
6956	1994 May 3	1200	1.6	0.01
6995	1995 Dec 26	300	1.7	0.19
7047	1994 May 2	195	1.6	0.02
7125	1994 May 6	600	2.5	0.01
7151	1994 May 6	1015	2.0	0.06
7199	1995 May 27	400	1.3	0.07
7204	1995 Feb 3	300	2.3	0.51
7232	1995 May 27	400	1.2	0.07
7261	1994 May 4	600	2.2	0.01
7278	1995 Dec 29	300	1.5	0.19
7306	1995 Dec 28	600	1.5	0.19
7323	1994 May 5	600	2.2	0.01
7356	1995 May 27	900	1.4	0.07
7399	1994 May 6	600	2.4	0.01
7408	1994 May 3	600	1.9	0.01
7490	1994 May 4	300	2.2	0.01
7524	1995 Dec 29	300	1.6	0.19
7534	1994 May 5	670	2.5	0.01
7559	1994 May 7	600	1.7	0.06
7577	1994 May 2	1200	1.9	0.02
7592	1994 May 4	45	2.6	0.01
7599	1996 May 11	600	1.0	0.02
7603	1994 May 5	420	2.2	0.01
7608	1994 May 6	1200	2.0	0.01

Table A.3. – Continued

UGC	date	$t_{\rm exp}$ sec	seeing $''$	$\sigma_{\rm phot}$ mag
(1)	(2)	(3)	(4)	(5)
7648	1994 May 7	60	2.0	0.06
7651	1994 May 7	60	2.0	0.06
7673	1996 May 11	600	1.5	0.02
7690	1994 May 3	600	1.9	0.01
7698	1994 May 5	1200	2.0	0.01
7723	1995 Feb 3	300	2.0	0.51
7831	1994 May 2	120	2.1	0.02
7853	1995 Dec 27	900	1.3	0.06
7861	1995 Dec 27	1800	1.2	0.07
7866	1994 May 3	600	2.1	0.01
7872	1995 May 28	600	2.0	0.04
7907	1995 Dec 29	300	1.6	0.19
7916	1994 May 4	1500	2.1	0.01
7949	1994 May 5	1200	1.9	0.01
7971	1995 Feb 3	600	2.2	0.51
8005	1994 May 6	600	1.8	0.01
8024	1994 May 7	600	1.8	0.06
8098	1994 May 3	660	1.9	0.01
8188	1994 May 4	600	2.2	0.01
8201	1994 May 7	600	2.4	0.06
8286	1995 Feb 3	300	1.8	0.51
8303	1995 May 28	600	1.3	0.07
8320	1994 May 3	600	2.0	0.01
8331	1994 May 5	600	1.7	0.01
8441	1995 May 29	600	1.7	0.04
8489	1995 May 29	600	2.0	0.04
8490	1994 May 2	360	2.2	0.02
8508	1995 May 28	600	1.6	0.07
8550	1994 May 3	600	1.8	0.01
8565	1995 May 29	600	3.0	0.04
8651	1994 May 4	600	1.7	0.01
8683	1994 May 5	1200	1.9	0.01
8760	1994 May 6	900	2.0	0.01
8837	1994 May 4	600	1.9	0.01
8892	1996 May 12	600	1.4	0.02
9018	1996 May 11	600	1.6	0.02
9128	1995 May 28	600	1.3	0.07
9211	1994 May 5	1200	2.2	0.01
9219	1995 May 28	600	1.5	0.07
9240	1994 May 5	1800	2.1	0.01
9405	1995 May 29	600	2.4	0.04
9426	1995 May 28	900	1.5	0.07
9769	1996 May 14	600	1.9	0.01
9906	1994 May 5	1380	2.3	0.01
9992	1995 May 29	600	2.1	0.04
10736	1996 May 12	600	1.4	0.02
10792	1996 May 12	1200	1.4	0.02
10806	1996 May 11	600	1.8	0.02
11283	1996 May 12	720	1.3	0.02
11557	1994 May 6	420	1.5	0.01
11707	1996 May 14	600	1.8	0.01
12048	1994 Dec 3	300	2.6	0.02
12060	1994 Dec 3	600	2.4	0.02
12212	1994 Dec 3	480	2.8	0.02
12554	1995 Dec 23	300	0.9	0.02
12632	1995 Dec 23	600	0.9	0.02
12732	1994 Dec 3	600	2.6	0.02

Table A.4. List of B-band observations

UGC	date	$t_{\rm exp}$ s	seeing $''$	$\sigma_{\rm phot}$ mag
(1)	(2)	(3)	(4)	(5)
731	23 Dec 1995	600	1.0	0.03
1281	24 Dec 1995	900	1.1	0.09
1501	24 Dec 1995	600	1.1	0.09
2800	23 Dec 1995	600	1.1	0.03
3060	24 Dec 1995	600	1.3	0.09
3137	5 Feb 1995	600	1.6	0.45
3144	24 Dec 1995	600	1.2	0.03
3273	25 Dec 1995	600	1.3	0.12
3317	24 Dec 1995	600	1.2	0.03
3371	24 Dec 1995	900	1.4	0.09
3384	26 Dec 1995	900	1.7	0.12
3390	26 Dec 1995	600	1.1	0.12
3475	27 Dec 1995	900	1.0	0.12
3647	26 Dec 1995	900	1.8	0.12
3698	27 Dec 1995	900	1.0	0.12
3851	28 Dec 1995	180	1.6	0.12
3860	26 Dec 1995	600	1.4	0.12
4274	26 Dec 1995	300	1.7	0.12
4278	28 Dec 1995	300	1.5	0.02
4305	28 Dec 1995	180	1.7	0.04
4325	24 Dec 1995	300	1.2	0.03
4660	24 Dec 1995	600	1.6	0.03
5040	26 Dec 1995	600	1.5	0.12
5336	24 Dec 1995	900	1.2	0.03
5829	3 Feb 1995	600	2.6	0.45
6151	26 Dec 1995	600	1.3	0.12
6713	3 Feb 1995	600	2.4	0.45
6912	3 Feb 1995	600	1.7	0.45
7199	27 May 1995	600	2.5	0.09
7232	27 May 1995	800	2.8	0.09
7356	27 May 1995	900	1.7	0.09
7399	28 May 1995	600	2.5	0.05
7534	5 May 1994	60	1.9	0.01
7577	2 May 1994	1200	2.2	0.02
7861	24 Dec 1995	1800	1.1	0.03
7872	28 May 1995	600	2.8	0.05
8303	28 May 1995	600	6.8	0.09
8441	29 May 1995	600	1.9	0.05
8489	29 May 1995	900	2.5	0.05
8508	28 May 1995	600	3.4	0.09
8565	29 May 1995	600	2.9	0.05
9128	28 May 1995	900	3.8	0.09
9219	29 May 1995	600	2.8	0.05
9992	29 May 1995	600	3.4	0.05
12554	23 Dec 1995	300	1.0	0.03
12632	23 Dec 1995	600	1.0	0.03

Table A.5. *R*-band isophotal and photometric parameters

UGC	ϵ	PA	m_{25}	$m_{\rm lim}$	$m_{\rm ext}$	$\mu_{\rm lim}$	$\mu_{\rm c}$	μ_0	M_R	$\sigma_{\rm phot}$	h	d_{25}	$d_{26.5}$	r_{20}	r_{50}	r_{80}
(1)	(2)	(3)	(4)	(5)	(6)	(7)	(8)	(9)	(10)	(11)	(12)	(13)	(14)	(15)	(16)	(17)
192[a]	0.474	133	9.75	9.93	9.79	24.08	21.35	20.76	-15.21	0.05	92.7	1015	–	74	145	239
731	0.506	73	13.50	13.52	13.29	24.95	21.86	22.24	-16.63	0.02	45.8	249	–	29	63	104
1249[b]	0.629	151	11.63	11.60	11.58	25.78	22.13	21.05	-17.94	0.22	56.4	396	463	42	91	144
1281	0.872	40	12.72	12.61	12.61	26.64	21.00	20.51	-16.17	0.02	45.9	359	582	41	79	133
1438[b]	0.347	87	12.70	12.65	12.65	27.62	19.59	19.52	-18.27	0.22	13.6	140	184	11	22	41
1501	0.774	1	11.70	11.65	11.63	26.10	21.28	20.65	-17.27	0.02	58.5	448	592	47	93	158
1547	0.000	90	14.02	13.74	13.70	26.50	21.30	21.63	-17.98	0.05	15.6	98	162	12	27	54
1551	0.105	119	13.63	13.49	13.45	27.37	21.25	21.74	-18.26	0.05	22.1	132	169	18	35	57
1865	0.152	65	14.03	13.90	13.58	25.46	22.39	22.59	-16.56	0.02	29.3	130	196	21	45	82
2014[b]	0.604	176	14.49	14.33	14.26	26.28	22.38	22.12	-15.86	0.22	26.2	136	196	20	40	64
2017	0.500	45	15.62	15.37	15.19	25.69	23.11	22.73	-16.02	0.05	21.1	90	169	16	32	51
2023	0.000	89	13.31	13.16	13.01	25.85	22.07	21.79	-17.20	0.02	25.3	152	214	20	42	77
2034	0.000	90	12.93	12.85	12.67	25.46	21.76	21.56	-17.45	0.05	25.5	155	220	21	42	77
2053	0.630	38	14.73	14.57	14.54	26.75	22.66	21.46	-16.02	0.05	19.3	124	169	19	34	54
2455	0.165	37	11.42	11.38	11.36	26.36	19.70	19.64	-18.47	0.05	23.2	231	298	18	38	69
2603[b]	0.588	64	14.68	14.54	14.44	25.97	21.85	21.99	-18.88	0.18	25.1	142	257	20	40	61
2800	0.604	106	13.46	13.31	13.28	26.26	20.14	20.69	-19.06	0.02	28.5	210	319	22	44	77
3056[b]	0.534	120	10.55	10.56	10.52	24.90	16.19	20.33	-17.34	0.22	57.9	500	–	16	35	83
3060	0.789	24	10.97	10.93	10.92	25.88	20.61	20.31	-17.39	0.07	77.8	708	907	63	129	227
3137[b]	0.765	74	13.2	12.9	12.9	27.1	20.9	22.7	-18.7	0.51	64.7	283	457	27	58	127
3144	0.516	113	13.84	13.73	13.69	26.49	21.28	21.27	-18.08	0.02	22.3	161	203	18	35	64
3273[a,b]	0.603	38	13.4	13.3	13.3	25.8	21.0	21.3	-17.1	0.51	25.1	178	249	17	38	69
3317	0.355	18	14.84	14.57	14.47	27.08	22.51	22.37	-17.24	0.02	21.8	111	150	17	36	58
3371	0.378	130	13.64	13.28	13.07	26.01	22.43	22.78	-17.74	0.07	52.6	213	339	38	79	134
3384[b]	0.000	135	14.51	14.49	14.44	25.17	21.21	21.25	-17.31	0.18	9.7	96	–	9	21	38
3390[a,b]	0.357	41	13.31	13.24	13.16	26.05	19.93	21.39	-18.67	0.18	22.5	140	182	15	33	58
3475	0.421	73	13.51	13.55	13.44	24.68	20.15	20.49	-17.06	0.05	18.4	158	–	15	30	49
3647[b]	0.000	34	14.06	13.83	13.69	26.05	22.12	22.18	-17.71	0.18	20.4	104	228	16	33	61
3698[b]	0.294	179	14.66	14.47	14.46	26.44	21.85	20.85	-15.42	0.18	10.3	80	133	11	19	35
3711	0.385	101	12.18	12.18	12.13	25.05	18.86	20.38	-17.76	0.01	21.9	183	–	12	26	53
3817[b]	0.000	90	15.34	14.94	14.76	26.15	23.15	22.54	-15.13	0.22	15.9	72	129	14	28	49
3851	0.642	28	11.02	10.92	10.89	25.76	21.82	21.44	-16.86	0.02	87.9	594	1034	77	135	246
3860[b]	0.482	24	14.48	14.33	14.29	26.57	23.23	21.60	-15.00	0.18	17.9	115	159	15	29	51
3966	0.000	90	14.56	14.40	14.14	25.88	23.14	22.24	-14.87	0.02	18.6	94	143	19	34	59
4173	0.397	138	14.30	13.58	13.37	26.56	22.37	23.77	-17.81	0.02	61.4	133	294	28	78	139
4274[b]	0.075	158	11.29	11.27	11.23	25.37	19.77	20.66	-17.95	0.18	23.2	185	257	15	23	46
4278	0.882	173	12.47	12.45	12.45	25.78	20.29	20.20	-17.73	0.02	45.4	348	454	34	68	112
4305	0.246	30	11.11	10.98	10.93	26.44	22.21	21.38	-16.78	0.01	59.7	389	565	56	105	175
4325	0.356	56	12.10	12.04	12.02	26.73	21.18	21.13	-18.10	0.02	35.9	241	304	28	55	91
4426[b]	0.303	3	14.62	14.32	14.23	27.13	22.73	22.64	-14.87	0.22	24.2	113	161	19	40	65
4483[b]	0.444	167	14.48	14.51	14.27	24.84	21.96	21.79	-13.59	0.18	19.2	101	–	15	25	46
4499	0.173	162	13.01	12.90	12.86	26.63	20.50	21.29	-17.78	0.02	21.5	149	203	15	36	62
4543	0.000	90	13.56	13.28	13.22	26.69	20.61	22.02	-19.24	0.05	23.0	123	205	15	36	71
4660	0.000	90	14.75	14.48	14.40	26.69	21.31	22.25	-18.21	0.02	13.9	71	113	9	21	41
4704	0.861	116	13.94	13.87	13.84	25.63	21.32	21.68	-16.23	0.02	43.3	246	345	32	63	100
4945	0.000	90	15.02	14.89	14.46	25.48	23.00	22.77	-14.67	0.02	18.4	73	143	15	30	57
5040	0.000	90	13.70	13.55	13.51	27.10	20.61	22.19	-20.31	0.05	23.0	115	151	15	32	53
5139	0.000	90	13.33	13.17	12.72	25.47	24.00	22.68	-16.47	0.01	42.4	182	291	46	81	140
5221	0.423	143	9.72	9.72	9.71	24.96	19.36	18.69	-18.61	0.02	36.1	451	–	38	69	114
5272	0.640	114	13.95	13.86	13.83	26.28	22.05	21.24	-15.11	0.01	21.5	142	201	19	36	57
5322[b]	0.612	63	7.70	7.70	7.69	25.24	-0.07	17.33	-21.23	0.18	54.5	956	–	43	89	166
5336	0.399	60	14.11	13.36	13.07	25.83	23.72	23.55	-14.79	0.02	70.6	184	416	54	108	167

Table A.5. – Continued

UGC	ϵ	PA	m_{25}	$m_{\rm lim}$	$m_{\rm ext}$	$\mu_{\rm lim}$	$\mu_{\rm c}$	μ_0	M_R	$\sigma_{\rm phot}$	h	d_{25}	$d_{26.5}$	r_{20}	r_{50}	r_{80}
(1)	(2)	(3)	(4)	(5)	(6)	(7)	(8)	(9)	(10)	(11)	(12)	(13)	(14)	(15)	(16)	(17)
5340	0.501	8	14.57	14.44	14.37	26.07	21.85	21.99	-14.57	0.01	18.9	103	169	13	27	48
5364	0.497	102	13.02	12.84	12.60	25.51	23.71	22.78	-14.15	0.01	69.3	276	455	57	102	165
5398	0.231	49	9.51	9.51	9.47	25.19	17.96	19.89	-18.43	0.01	51.8	478	–	25	65	132
5414	0.416	38	12.59	12.48	12.47	27.82	21.85	21.18	-17.55	0.02	30.4	210	270	27	53	85
5455	0.440	147	15.85	15.37	15.33	27.22	23.02	22.47	-16.54	0.05	15.1	68	119	13	26	47
5478	0.000	42	15.19	15.04	14.57	25.42	22.62	22.91	-16.80	0.07	18.7	70	115	15	30	58
5612[b]	0.193	166	12.4	12.3	12.2	25.7	20.9	21.4	-18.6	0.51	32.0	205	251	24	51	86
5666[b]	0.630	48	10.70	10.78	10.65	24.69	22.12	22.14	-17.23	0.18	137.8	779	–	111	217	315
5688[b]	0.360	133	13.42	13.33	13.22	25.89	21.32	22.00	-19.18	0.06	28.7	162	214	21	46	76
5706	0.573	100	16.38	15.84	15.72	26.45	23.23	23.35	-16.24	0.07	21.7	71	129	17	33	53
5721	0.504	96	12.60	12.59	12.58	25.40	19.15	19.47	-16.58	0.02	13.6	143	179	11	23	40
5740[b]	0.358	123	13.9	13.8	13.8	26.5	21.4	21.7	-16.6	0.51	19.3	122	166	15	32	55
5764[b]	0.474	48	15.2	14.9	14.9	27.0	22.2	21.9	-14.9	0.51	14.0	81	123	12	24	43
5829	0.000	81	12.86	12.59	12.46	26.39	22.60	22.43	-17.33	0.01	38.8	188	296	33	65	115
5846	0.142	90	15.05	14.65	14.52	26.90	23.32	22.69	-16.08	0.02	18.9	78	126	16	32	54
5860[b]	0.462	92	12.60	12.58	12.57	26.00	17.96	19.62	-18.63	0.18	11.6	119	165	5	13	30
5918	0.508	83	14.91	14.22	14.05	26.15	23.28	23.43	-15.38	0.01	46.2	120	310	31	66	114
5935[b]	0.609	97	12.05	11.98	11.97	27.06	17.78	20.79	-20.14	0.06	31.0	244	326	11	33	77
5986	0.730	40	11.13	11.07	11.07	26.59	19.17	20.00	-18.63	0.02	45.8	419	567	34	72	127
6016[b]	0.300	56	14.8	14.6	14.5	26.2	21.7	22.6	-17.6	0.51	19.4	89	144	13	29	51
6021[b]	0.000	116	12.42	12.41	12.39	25.69	18.92	19.30	-20.14	0.18	10.1	106	132	9	19	32
6024	0.626	66	11.76	11.73	11.73	26.00	19.04	19.12	-20.10	0.01	19.3	207	353	15	32	56
6126[b]	0.825	164	12.52	12.50	12.49	25.32	19.73	20.16	-17.26	0.06	32.1	307	–	23	52	94
6151[b]	0.000	90	14.24	13.99	13.91	27.02	22.00	22.24	-17.27	0.18	18.2	98	142	15	32	54
6161[b]	0.597	49	13.53	13.44	13.41	26.31	20.59	21.41	-17.14	0.06	24.0	160	217	15	36	64
6251[b]	0.112	13	14.85	14.66	14.52	25.97	22.07	22.37	-16.08	0.18	14.7	70	106	9	21	40
6406	0.150	167	12.50	12.38	12.31	26.40	17.38	23.28	-19.35	0.02	39.1	124	231	4	11	49
6446	0.161	26	12.17	12.10	12.05	26.23	20.30	21.17	-18.35	0.02	28.5	201	273	19	43	80
6456[b]	0.547	166	14.73	14.43	14.39	26.79	21.69	22.41	-13.05	0.18	22.5	106	177	14	30	61
6565	0.272	162	11.26	11.21	11.19	26.00	19.71	20.75	-16.34	0.01	32.3	253	364	16	36	78
6628	0.000	90	12.34	12.17	12.08	26.62	20.95	21.79	-18.85	0.01	35.8	200	294	28	56	102
6682[b]	0.190	24	13.97	13.70	13.56	26.18	22.08	22.42	-17.47	0.18	27.0	126	200	21	46	78
6817	0.478	65	13.10	13.03	12.84	25.36	22.64	22.38	-15.18	0.01	48.5	230	346	37	70	118
6840	0.194	72	13.52	13.30	13.22	26.59	20.88	21.83	-17.77	0.02	26.3	152	223	16	46	83
6912[b]	0.315	143	13.1	13.1	13.1	24.9	21.0	20.8	-18.8	0.51	16.4	164	–	14	30	56
6917[b]	0.439	125	11.6	11.6	11.6	25.5	20.0	20.7	-19.6	0.51	38.6	262	302	28	56	92
6944	0.547	25	12.21	12.21	12.20	25.32	18.00	19.52	-21.19	0.02	17.0	179	213	12	27	52
6955	0.613	67	13.06	12.93	12.90	26.12	22.40	22.13	-17.42	0.01	50.1	252	342	37	69	112
6956	0.169	142	14.42	14.00	13.81	26.89	22.09	23.24	-17.19	0.01	33.4	114	186	21	49	89
6995[b]	0.100	1	12.20	12.15	12.15	27.70	18.86	19.72	-19.65	0.18	13.0	126	170	9	19	37
7047	0.155	34	12.67	12.56	12.50	26.24	21.61	21.40	-15.22	0.02	27.0	171	235	23	43	75
7125	0.773	85	13.21	13.13	13.12	26.23	21.04	21.19	-18.34	0.01	34.2	252	335	25	52	97
7151[b]	0.770	102	12.10	12.07	12.05	25.56	20.50	20.70	-15.67	0.06	43.7	372	508	34	74	135
7199	0.345	12	12.69	12.60	12.58	26.43	20.66	20.92	-15.14	0.07	21.8	165	233	16	33	62
7204[b]	0.806	134	12.3	12.3	12.3	26.5	20.6	19.8	-19.3	0.51	30.4	286	398	29	54	92
7232	0.178	65	12.48	12.43	12.41	25.73	20.81	19.96	-15.31	0.07	14.8	142	206	15	28	47
7261	0.000	121	12.29	12.18	12.13	26.78	20.35	21.85	-17.71	0.01	35.1	204	265	21	50	88
7278[b]	0.063	20	9.45	9.41	9.39	26.51	18.90	20.15	-18.33	0.18	53.3	481	631	32	74	153
7306[b]	0.733	160	9.65	9.57	9.55	26.08	21.28	21.26	-17.87	0.18	174.6	1212	1793	139	282	478
7323	0.246	29	10.77	10.69	10.64	25.96	20.68	20.91	-18.90	0.01	53.7	382	527	42	86	145
7356	0.330	159	14.79	14.59	14.52	26.37	22.50	21.82	-13.20	0.07	15.1	88	130	15	28	45
7399	0.358	126	12.57	12.52	12.50	26.18	19.62	20.25	-17.12	0.01	17.8	155	206	14	30	52

Table A.5. – Continued

UGC	ϵ	PA	m_{25}	$m_{\rm lim}$	$m_{\rm ext}$	$\mu_{\rm lim}$	$\mu_{\rm c}$	μ_0	M_R	$\sigma_{\rm phot}$	h	d_{25}	$d_{26.5}$	r_{20}	r_{50}	r_{80}
(1)	(2)	(3)	(4)	(5)	(6)	(7)	(8)	(9)	(10)	(11)	(12)	(13)	(14)	(15)	(16)	(17)
7408	0.279	96	13.22	13.08	13.02	25.99	21.60	21.56	-16.60	0.01	24.2	155	234	20	40	71
7490	0.000	90	12.44	12.31	12.25	26.54	21.31	21.33	-17.40	0.01	27.3	180	257	24	47	81
7524[b]	0.368	131	9.76	9.65	9.58	26.04	20.97	21.70	-18.14	0.18	135.1	867	1111	116	225	395
7534	0.000	36	13.84	13.75	13.46	25.59	0.00	22.45	-16.19	0.01	24.8	120	167	25	42	76
7559[b]	0.476	157	14.14	13.87	13.87	25.69	22.80	23.08	-13.66	0.06	44.6	157	283	26	51	81
7577	0.577	127	12.25	12.14	12.10	26.08	22.28	21.56	-15.62	0.02	50.8	318	451	43	82	137
7592	0.210	66	9.27	9.26	9.24	25.25	18.38	20.09	-18.48	0.01	50.5	454	–	26	57	112
7599	0.474	126	14.51	14.39	14.34	27.01	22.04	21.66	-13.38	0.02	16.9	97	128	14	27	43
7603	0.667	17	12.36	12.32	12.31	26.38	20.09	19.61	-16.88	0.01	20.8	204	272	20	37	63
7608	0.000	90	13.63	13.29	13.19	27.15	22.26	22.63	-16.43	0.01	30.4	135	217	22	49	87
7648[b]	0.313	176	11.66	11.64	11.62	25.36	19.70	19.71	-17.64	0.06	18.8	192	264	14	29	55
7651[b]	0.534	120	9.42	9.41	9.40	25.88	18.30	18.68	-20.22	0.06	40.9	447	562	30	67	114
7673	0.300	35	14.92	14.54	14.48	27.15	22.73	22.42	-15.16	0.02	19.2	89	145	17	33	57
7690	0.000	24	12.56	12.53	12.51	26.42	19.98	19.91	-16.98	0.01	11.8	121	148	10	21	40
7698	0.466	168	13.32	12.94	12.84	26.15	23.26	22.53	-14.90	0.01	50.4	226	369	46	86	142
7723[b]	0.284	117	11.6	11.6	11.6	25.2	19.5	20.6	-18.7	0.51	25.4	206	–	15	32	63
7831	0.535	119	9.93	9.93	9.92	25.47	18.99	18.70	-18.66	0.02	32.7	402	499	28	55	97
7853[b]	0.226	10	10.39	10.38	10.35	25.25	19.17	19.75	-19.11	0.06	32.1	314	–	26	61	101
7861	0.000	90	12.00	11.84	11.81	27.89	19.81	23.38	-17.96	0.07	44.8	134	257	12	25	52
7866	0.270	10	13.40	13.25	13.18	26.09	22.08	21.79	-15.23	0.01	24.7	153	223	20	42	73
7872	0.324	177	14.75	14.75	14.44	24.99	22.05	22.58	-18.02	0.04	21.2	94	–	12	29	51
7907[b]	0.846	35	10.64	10.51	10.51	26.27	19.85	20.53	-18.98	0.18	96.0	785	1300	68	157	299
7916	0.700	170	14.99	14.92	14.70	25.44	23.53	23.04	-14.93	0.01	42.0	153	222	27	50	82
7949	0.507	74	14.34	14.13	14.05	26.35	23.08	22.28	-14.37	0.01	28.0	145	217	26	47	78
7971[b]	0.200	35	12.6	12.6	12.5	25.9	21.2	21.0	-17.1	0.51	23.0	165	209	20	40	68
8005	0.643	35	11.70	11.47	11.47	26.27	20.26	20.41	-20.25	0.01	36.8	381	909	33	76	185
8024[b]	0.463	33	13.88	13.69	13.64	26.35	22.57	21.77	-14.78	0.06	24.5	142	218	23	41	70
8098	0.647	23	12.60	12.50	12.47	26.30	21.50	21.34	-18.07	0.01	42.0	272	376	32	64	112
8188	0.106	90	11.19	11.09	10.99	25.88	22.04	21.20	-17.37	0.01	52.0	352	489	53	101	162
8201[b]	0.511	94	12.85	12.71	12.68	26.97	22.71	21.08	-15.79	0.06	32.4	237	314	39	68	105
8286[b]	0.759	28	11.3	11.3	11.2	25.6	19.6	19.4	-17.2	0.51	34.4	346	431	30	59	101
8303	0.000	90	13.16	12.99	12.94	26.93	21.95	21.31	-18.24	0.07	18.9	136	191	17	33	65
8320	0.380	150	12.53	12.47	12.38	25.36	22.35	21.49	-16.47	0.01	35.3	230	350	31	59	99
8331	0.691	139	13.94	13.80	13.77	26.27	22.24	21.63	-15.08	0.01	27.8	173	248	23	45	77
8441	0.209	70	14.05	13.79	13.71	27.85	22.18	22.47	-17.80	0.04	25.6	119	175	19	40	69
8489	0.622	104	14.04	13.95	13.93	27.19	20.56	21.27	-17.58	0.04	18.0	124	163	12	27	48
8490	0.398	175	11.22	11.19	11.18	26.06	19.76	19.95	-17.28	0.02	29.0	285	360	24	50	90
8508	0.458	119	13.43	13.27	13.27	27.83	21.64	20.85	-14.57	0.07	18.6	140	201	18	34	59
8550	0.809	169	13.12	13.05	13.05	26.37	20.34	20.16	-15.57	0.01	24.2	223	327	21	41	74
8565	0.304	179	13.11	12.95	12.93	26.74	20.93	21.13	-15.65	0.04	21.4	151	230	19	38	66
8651	0.419	76	13.95	13.75	13.72	27.49	22.63	21.70	-15.13	0.01	22.4	139	188	22	41	67
8683	0.000	90	14.40	13.82	13.78	29.84	22.28	22.49	-16.72	0.01	20.5	83	176	15	35	76
8760	0.640	33	13.94	13.75	13.74	27.28	22.32	21.27	-15.11	0.01	23.0	156	228	24	44	72
8837	0.717	22	12.97	12.88	12.83	25.41	21.91	21.83	-15.71	0.01	49.5	284	397	39	76	123
8892	0.479	52	14.33	14.02	14.00	28.22	21.86	22.01	-18.31	0.02	22.2	122	179	19	40	70
9018	0.277	90	13.64	13.46	13.44	26.92	21.54	21.33	-15.99	0.02	18.0	113	181	14	28	51
9128	0.258	19	14.10	13.97	13.89	26.15	22.76	21.54	-14.33	0.07	17.2	110	154	18	32	52
9211	0.212	107	14.61	14.51	14.29	25.93	22.56	22.38	-16.21	0.01	19.4	93	132	15	31	54
9219	0.496	99	13.13	13.07	13.06	27.25	20.70	20.89	-17.34	0.07	21.0	154	193	17	34	56
9240	0.144	90	12.61	12.53	12.49	26.09	21.60	20.80	-15.78	0.01	20.6	160	232	20	37	64
9405	0.442	147	14.09	13.91	13.85	26.38	22.00	22.18	-15.55	0.04	24.6	140	193	19	42	70
9426	0.000	90	15.34	15.03	14.91	27.13	21.84	22.63	-17.96	0.07	14.0	63	96	10	22	40

Table A.5. – Continued

UGC	ϵ	PA	m_{25}	$m_{\rm lim}$	$m_{\rm ext}$	$\mu_{\rm lim}$	$\mu_{\rm c}$	μ_0	M_R	$\sigma_{\rm phot}$	h	d_{25}	$d_{26.5}$	r_{20}	r_{50}	r_{80}
(1)	(2)	(3)	(4)	(5)	(6)	(7)	(8)	(9)	(10)	(11)	(12)	(13)	(14)	(15)	(16)	(17)
9769	0.353	9	13.24	13.10	13.01	26.38	20.69	22.24	-18.10	0.01	33.5	170	238	18	44	83
9906	0.307	51	11.98	11.86	11.81	26.08	18.73	22.73	-18.87	0.01	45.5	179	310	9	19	66
9992	0.319	148	14.53	14.26	14.24	27.65	21.72	21.75	-15.89	0.04	15.9	90	149	13	26	49
10310	0.298	108	13.24	13.11	13.07	26.62	21.55	21.66	-17.90	0.02	24.9	158	217	20	42	71
10736	0.727	156	13.81	13.75	13.73	25.95	21.11	21.13	-16.71	0.02	27.1	183	229	21	43	68
10792	0.339	94	16.07	16.00	15.77	25.26	22.78	22.27	-16.05	0.02	10.9	54	–	9	17	29
10806	0.490	81	12.87	12.83	12.83	27.10	19.85	19.94	-18.45	0.02	15.1	134	164	13	27	44
11283	0.000	90	12.94	12.89	12.84	25.88	19.47	20.84	-19.78	0.01	16.8	121	155	12	25	43
11557	0.187	106	12.90	12.88	12.82	25.54	20.00	20.73	-19.71	0.01	26.2	171	198	17	34	53
11707	0.599	56	12.97	12.93	12.77	25.62	20.66	22.08	-18.60	0.02	58.0	293	401	29	73	120
11861	0.392	125	12.25	12.51	12.23	23.84	19.37	20.87	-20.79	0.02	52.9	348	–	31	60	92
12048	0.251	125	12.21	12.16	12.14	26.82	20.30	20.05	-19.13	0.02	19.0	170	221	16	31	54
12060	0.000	146	13.43	13.32	13.23	26.11	21.10	21.56	-17.95	0.02	20.8	145	195	15	36	64
12212	0.300	110	14.36	14.24	14.15	26.06	21.51	21.81	-16.94	0.02	17.8	115	154	14	30	52
12554	0.790	168	10.67	10.62	10.62	26.67	19.34	19.90	-19.44	0.02	73.2	674	861	55	125	219
12632	0.441	20	12.77	12.74	12.34	25.08	21.72	22.88	-17.14	0.01	84.7	339	–	52	112	186
12732	0.184	6	13.04	12.73	12.69	26.93	21.51	22.14	-18.01	0.01	35.4	181	308	25	55	104

Table A.6. *B*-band isophotal and photometric parameters

UGC	ϵ	PA	m_{25}	$m_{\rm lim}$	$m_{\rm ext}$	$\mu_{\rm lim}$	$\mu_{\rm c}$	μ_0	M_R	$\sigma_{\rm phot}$	h	d_{25}	$d_{26.5}$	r_{20}	r_{50}	r_{80}
(1)	(2)	(3)	(4)	(5)	(6)	(7)	(8)	(9)	(10)	(11)	(12)	(13)	(14)	(15)	(16)	(17)
731	0.506	73	15.12	14.43	14.14	25.78	22.98	23.27	-15.78	0.03	50.5	154	284	34	70	110
1281	0.872	40	13.63	13.50	13.49	26.92	21.74	21.10	-15.29	0.09	41.9	290	405	39	75	121
1501	0.774	1	12.49	12.37	12.36	27.19	21.99	21.29	-16.54	0.09	55.8	376	497	45	90	151
2800	0.604	106	15.61	15.08	15.06	28.35	21.97	22.16	-17.28	0.03	25.5	137	194	23	43	70
3060	0.789	24	12.19	11.98	11.97	27.96	21.76	21.45	-16.34	0.09	81.3	540	773	65	135	237
3137[b]	0.765	74	15.1	14.7	14.7	27.0	22.7	22.1	-16.9	0.45	29.4	156	240	25	47	82
3144	0.516	113	15.32	14.87	14.84	27.19	22.35	22.36	-16.93	0.03	21.1	100	170	18	35	63
3273[a,b]	0.720	42	15.00	14.68	14.64	27.00	22.00	22.74	-15.79	0.12	32.3	140	218	21	47	81
3317	0.355	18	16.71	15.57	15.37	27.26	23.59	23.55	-16.34	0.03	25.0	65	133	20	39	64
3371	0.378	130	16.10	14.50	14.15	26.54	23.89	23.98	-16.66	0.09	57.0	103	265	42	82	138
3384[b]	0.000	135	16.41	15.53	15.27	26.60	22.44	23.37	-16.48	0.12	18.1	50	109	12	29	52
3390[a,b]	0.357	41	15.51	14.99	14.95	27.91	21.58	22.62	-16.88	0.12	18.6	82	132	16	35	58
3475	0.421	73	18.67	16.45	16.37	28.23	23.23	23.11	-14.13	0.12	17.5	44	109	17	32	50
3647[b]	0.000	34	15.04	13.95	13.94	28.21	22.84	22.82	-17.46	0.12	18.8	76	128	22	60	107
3698[b]	0.294	179	15.74	15.35	15.33	26.53	22.97	21.72	-14.55	0.12	10.1	61	114	11	20	36
3851	0.642	28	11.74	11.59	11.54	26.07	22.54	22.07	-16.21	0.12	85.7	478	675	74	119	218
3860[b]	0.482	24	15.56	15.15	15.09	27.07	23.05	22.48	-14.20	0.12	18.9	79	136	16	29	52
4274[b]	0.075	158	12.49	12.42	12.38	26.27	20.95	21.90	-16.80	0.12	22.4	127	195	14	22	40
4278	0.900	172	12.07	12.07	12.06	25.14	19.73	19.87	-18.12	0.02	50.7	396	–	37	76	119
4305	0.246	30	11.86	11.67	11.55	26.70	22.94	22.28	-16.16	0.04	68.1	349	467	60	115	184
4325	0.356	56	13.14	12.98	12.87	27.37	22.27	22.16	-17.25	0.03	38.8	193	254	31	58	96
4660	0.000	90	16.11	15.38	15.25	27.56	22.55	23.41	-17.36	0.03	16.4	46	96	10	25	47
5040	0.000	90	15.23	14.73	14.42	27.57	21.95	23.49	-19.40	0.12	26.4	76	124	19	40	129
5336	0.399	60	15.82	14.40	14.24	27.14	24.19	23.94	-13.62	0.03	47.8	89	228	37	75	125
5829[b]	0.000	58	13.1	12.7	12.6	26.8	22.4	22.7	-17.2	0.45	40.8	179	274	35	69	118
6151[b]	0.000	90	15.50	14.88	14.79	28.14	23.18	23.11	-16.39	0.12	18.3	66	112	16	31	53
6713[b]	0.179	121	14.3	14.2	14.1	26.8	21.9	22.0	-17.0	0.45	17.0	92	131	15	28	47
6912[b]	0.315	143	14.2	13.8	13.8	27.6	21.7	21.2	-18.1	0.45	12.6	112	195	14	33	70
7199	0.345	12	13.78	13.60	13.58	27.27	21.34	21.82	-14.14	0.09	19.9	115	176	14	27	54
7232	0.178	65	13.36	13.23	13.22	27.37	21.51	20.58	-14.50	0.09	13.3	107	158	14	26	43
7356	0.330	159	16.46	15.75	15.66	27.36	23.71	23.21	-12.06	0.09	16.7	56	99	16	29	48
7399	0.410	126	13.42	13.28	13.28	28.49	20.34	20.93	-16.34	0.05	18.4	138	188	16	34	57
7534	0.000	36	14.47	14.16	13.67	25.60	22.36	23.41	-15.98	0.01	34.1	102	177	22	53	137
7577	0.577	127	13.25	12.92	12.90	27.63	22.85	22.21	-14.82	0.02	46.0	232	373	41	77	137
7861	0.000	90	13.10	12.89	12.85	28.17	20.61	24.02	-16.92	0.03	38.4	95	173	12	25	50
7872	0.324	177	16.03	15.48	15.32	26.52	22.83	23.35	-17.14	0.05	19.8	61	117	13	29	51
8303	0.000	90	14.27	13.87	13.82	27.89	22.93	22.23	-17.36	0.09	19.4	91	159	18	33	63
8441	0.209	70	15.31	14.61	14.48	27.90	23.35	23.40	-17.03	0.05	27.8	83	154	21	44	75
8489	0.622	104	14.83	14.66	14.64	27.71	21.42	21.92	-16.87	0.05	17.6	103	145	12	27	47
8508	0.458	119	14.16	14.06	13.99	25.94	22.18	21.52	-13.85	0.09	18.4	112	167	16	31	50
8565	0.304	179	14.09	13.83	13.81	27.52	21.39	22.08	-14.77	0.05	21.5	112	172	16	34	60
9128	0.258	19	14.92	14.56	14.55	28.67	23.28	22.10	-13.67	0.09	16.0	85	128	17	30	51
9219	0.496	99	14.09	13.93	13.89	27.71	21.72	21.93	-16.51	0.05	23.2	127	172	19	37	61
9992	0.319	148	15.53	15.11	15.07	27.42	22.62	22.57	-15.94	0.05	15.9	71	118	13	26	48
12554	0.790	168	11.79	11.68	11.67	26.76	20.54	21.10	-18.39	0.03	75.4	568	744	60	132	221
12632	0.441	20	15.27	13.39	13.25	28.64	22.82	24.03	-16.23	0.03	94.3	150	398	61	125	216

Appendix B: Images and surface brightness profiles

The next pages show an overview of the images, surface brightness profiles and isophotal fits for the 171 late-type dwarf galaxies in the sample. For each galaxy one row with three panels is shown.

The first panel gives the R-band image. All images have been put on a common grayscale using the calibration described in Sect. 4, and without correcting for Galactic foreground extinction. On the top left of each panel the UGC number is given, along with at most one other common name (either NGC or DDO). In the lower left a yardstick is shown, where the size depends on the scale of the galaxy. This size is shown above the yardstick and represents 1, 2, 5 or 10 kpc. The white cross near the center of the galaxy gives the adopted center from the isophotal fits (see Sect. 5). The ellipse indicates the orientation parameters, derived from the isophotal fits, that were adopted for each galaxy and that were used to derive the radial surface brightness profile.

The second panel presents the radial surface brightness profile. On the top right the morphological type, the absolute R-band magnitude and the conversion between arcseconds and parsecs are given. The arrow on the left side indicates the 3σ above sky level. The radial surface brightness profile has not been corrected for Galactic foreground extinction. The radial scale is measured along the major axis.

The third panel gives the results from the isophotal fits with all parameters (center, position angle and ellipticity) free. Note that these are not the data from which the final orientation parameters were derived. These were derived in several steps as described in Sect. 5. Within this panel there are four subpanels. Clockwise from the top left these show the variation of ellipticity, position angle, y-position and x-position of the center with radius. The dotted line in each panel gives the adopted value for the plotted parameter.

Full version with figures in this appendix can be downloaded from:
http://www.robswork.net/publications/WHISPII.ps.gz